An investigation into the effects of heart disease on flow waveform indices

by

Shawn T. Samuelson

A Thesis Submitted to the

Graduate Faculty in Partial Fulfillment of the

Requirements for the Degree of

MASTER OF SCIENCE

Interdepartmental Program: Biomedical Engineering
Major: Biomedical Engineering

Iowa State University
Ames, Iowa
1995

TABLE OF CONTENTS

LIST OF TABLES

LIST OF FIGURES

ACKNOWLEDGMENTS

I would like to express my deepest gratitude to my major professor Dr. Thomas Rogge, for his guidance, encouragement, patience and especially his time and moral support. I am also thankful to my other committee members, Dr. Donald Young and Dr. Patrick Patterson, for their helpful suggestions in refining this paper, and to Dr. Mary Helen Greer for showing her faith in me time and time again. I would like to thank my friends and family members for their moral support and encouragement. Very special gratitude to my wife Jodi for her love and understanding of all the effort that goes into producing a thesis. A special thanks to Sutikno Wirogo, Charles Randall, and Brian Frake for their generous help throughout the course of this work.

All computations were done on Project Vincent using a DEC 3000 model 300L AXP workstation at the Iowa State University Computation Center.

CHAPTER 1. INTRODUCTION

Background

Arterial or cardiovascular diseases in humans have been a major concern in the United States for decades due to their high fatality rate. One major type of arterial disease is arteriosclerosis, which is the thickening or hardening of the arterial wall leading to loss of elasticity. A second major type of arterial disease, atherosclerosis, causes a build up of atheromatous plaque on the arterial wall. The plaque begins to extend into the lumen of the artery and narrows the area of the vessel (creating a stenosis) so that passage of blood becomes more difficult and the local flow patterns are changed. The turbulence and separation in the flow after the stenosis can trigger further plaque deposition as well as thrombus formation and development of an embolism, while the pressure drop across the stenosis will decrease tissue perfusion. The vascular beds supplied by arteries can usually compensate enough to allow adequate circulation for normal tissue perfusion, but for severe stenosis the beds cannot vasodilate further and resistance increases at a nonlinear rate (Stergiopulos et al., 1992). Extreme occlusion (>75%) of a coronary artery can possibly cause myocardial infarction and congestive heart failure (if the left ventricle is affected), while extreme occlusion of a carotid artery reduces blood circulation to the brain which may lead to a stroke. If blood circulation to peripheral tissue is severely reduced

then gangrene may set in and the tissue may die. Thus, early detection of stenosis would obviously be very beneficial to allow physicians time to begin preventative pharmacologic treatments on the patient rather than having to perform a higher risk and more expensive surgery after the fact.

Common cardiovascular diseases include hypertension, aortic valvular stenosis (AS), aortic regurgitation or insufficiency (AI), and a combination of aortic stenosis and regurgitation (AS/AI). Hypertension is a sustained elevation of the systemic arterial pressure. Even though hypertension is not an immediate cause of death, it is responsible for many other diseases such as stroke. The major cause of cardiac murmurs is disease of the heart valves. Aortic valvular stenosis is the condition when a valve is narrowed and blood flow through it is accelerated and turbulent. Aortic regurgitation, the loudest murmur, is the abnormality when the aortic valve is incompetent and blood flows back through it, again through a narrow orifice that accelerates flow. The systolic or diastolic timing of a murmur due to a stenosis or regurgitation of any particular valve can be predicted by the mechanical events of the cardiac cycle. In the case of AS, the timing of the murmur would be during systole, and in the case of AI, during diastole.

Hemodynamics is the study of blood in motion and is very useful in analyzing various blood flow related problems in the human body. Blood flow can be modeled in simple terms as a fluid flowing through a tube. Mathematical models have become quite accurate in reproducing pressure and flow waveforms in both normal and diseased conditions. As technology has developed it has become possible to simulate more accurately arterial pressure and flow waveforms. Also the conditions of the flow can be easily changed and recalculated much more rapidly with the aid of a model,

so that the need for invasive studies may eventually be reduced. Thus, from mathematical and computational models and past in vivo studies, it will be feasible to more accurately diagnose a patient with a diseased heart valve or to locate a severe arterial occlusion from blood pulse traces.

In a previous study, most of the major arteries of the systemic circulation have been computationally modeled using finite element and finite difference methods (Stergiopulos et al., 1992). The finite difference code used by Stergiopulos and modified by Brian C. Frake and me will be utilized in this study to calculate commonly used indices for normal heart conditions as well as for diseased heart conditions.

CHAPTER 2. LITERATURE REVIEW

Anatomic Considerations

The blood vessels of the body are considered a closed transport system of varying sized tubular ducts that allows blood to move from the heart to the tissues and then return to the heart. The motion of blood through the vessels is primarily provided by the pumping action of the heart. In the systemic circulation additional forward motion is provided by diastolic recoil of the walls of the artery, compression of the veins during exercise by the skeletal muscles, and the negative pressure in the thorax during inspiration. Blood is critical to continual cellular metabolism and tissue survival. It functions as an oxygen and nutrient supplier to the tissues, temperature regulator, and hormone distributor. Thus, it is important that flow is continuous and not restricted. In developed and industrialized nations, cardiovascular diseases and disorders are a leading cause of death, so it is important that signs of these diseases or disorders are detected early to avert a possible fatal flow failure. Since the focus of this study is the arterial system, where failures commonly occur, the remainder of this section will examine the anatomy and characteristics of arteries, arterioles, and capillaries in the systemic circulation.

The systemic system begins with the left ventricle of the heart and the aorta. From there, blood is pumped through the arteries and arterioles to the capillaries

where the blood equilibrates with the interstitial fluid. After equilibration the blood then drains through venules into the veins and back to the right atrium. The walls of the arteries of the systemic circulation are composed of an outer layer of connective tissue, a middle layer of smooth muscle, and an inner layer of endothelium and underlying connective tissue. The proportions of these layers varies throughout the systemic system. The larger diameter arteries and aorta contain a higher percentage of elastic tissue than the arterioles, which contain more smooth muscle. These larger arteries promote flow by expanding during systole and recoiling during diastole, while the arterioles are the major site of blood flow resistance. Small variances in arteriole caliber cause large variances in the total peripheral resistance, and will be noted in the computational model. Branching out from the arterioles are smaller vessels called capillaries made only of one layer thick endothelial cells. Their total area in an adult exceed 6300 m^2, and each capillary cross sectional area just permits the passage of one red blood cell at a time (Ganong, 1991). It is in these vascular beds that most oxygen, nutrient, hormone, and temperature transport takes place.

In a young adult, the arteries in the body are very compliant and readily expand with an increase in blood flow and pressure. The pressure wave that is created during systole travels at a much higher velocity than that of blood pumped through the systemic circulation during systole and expands the arteries as it travels. This expansion is called the *pulse* and can be palpated externally at various points on the body. A typical pulse velocity for a young adult is 4 m/s in the aorta, 8 m/s in the large arteries, and 16 m/s in the small arteries (Ganong, 1991). With increasing age, the arteries become more rigid which as a result quickens the pressure wave velocity traveling through the arteries. Examining the atrial pressure waveform, one

can determine the five phases of the cardiac cycle as a function of time: atrial systole, isovolumetric ventricular contraction, ventricular ejection, isovolumetric ventricular relaxation, and ventricular filling. Also, the point at which the aortic valve opens and closes can be determined.

Biophysical Considerations

Experimental Methods

Before the advent of non-invasive flow meters and pressure transducers, blood flow could only be directly measured experimentally by cannulating a blood vessel. This obviously had serious limitations, so non-invasive methods of measuring the flow velocity through arteries have been developed. The most common flow meter devices used today are the *Doppler flow meter* and the *electromagnetic flow meter*. The principle behind the electromagnetic flow meter is that blood acts like a conductor and, if placed in a magnetic field, will produce a detectable voltage whose magnitude is proportionate to the flow volume speed. The Doppler flow meter uses the Doppler effect to determine the rate at which blood is flowing through the vessel. This is accomplished by sending diagonal ultrasonic waves from an upstream crystal into a vessel. These are reflected from the blood cells and picked up by a second, downstream crystal. The reflected wave frequency is higher by an amount proportionate to the rate of flow toward the second crystal because of the Doppler effect (Ganong, 1991). Other indirect methods of measuring the blood flow in specific parts of the body, such as cerebral or renal blood flow, or extremities include adaptations of the Fick principle and indicator dilution techniques, and plethysmography. Thus, from these experimental techniques flow waveform data can be determined in various parts

of the body and can be coupled with different assessment indices to deduce the flow situation along pertinent arteries.

Mathematical and Computational Methods

Blood kinematics through arteries originally were modeled as an ideal fluid (non-viscous and incompressible) flowing through a rigid tube. Arteries are anything but rigid, except in specialized cases, and blood is a 2-phase system of liquid (plasma) and cells (primarily, erythrocytes). From the basic principles of conservation of mass and conservation of momentum, other theories began to be formed. A brief history of hemodynamic mathematical models will be discussed here as well as previous computational fluid dynamic models used in arterial modeling.

The Foundation of Hemodynamics In 1773, Stephan Hales tried to describe the distensible properties of the arteries. He believed the arteries to be elastic reservoirs which collect blood during systole by stretching and then discharge the blood during diastole via the recoil of the walls which causes the continuous forward motion of blood. In effect, he postulated that the vessels transformed the discontinuous blood flow due to the pumping of the heart into steady flow. In 1899, Otto Frank continued Hales train of thought and produced the *windkessel theory*, which was the first lumped-parameter, time-domain based model. It took into consideration the resistance and capacitance of vessels and could be modeled as an electrical network called a *transmission line* (Noordergraaf, 1963) expressed by the following equation:

$$Q = \frac{1}{k}\frac{dp}{dt} + \frac{p}{R} \tag{2.1}$$

where Q is blood flow, p is systemic pressure, R is resistance, and k is the elastic modulus of the vessel. The electrical model, where the resistance and capacitance are connected in parallel, has been very beneficial in explaining the relationship between flow from the heart and pressure throughout the system as a function of time. Also from this model, the stroke volume of the heart could be estimated accurately.

Unfortunately, the windkessel theory makes the assumption that pressure wave propagation in the arterial system travels at an infinite velocity, thus giving erroneous pressure-flow relations during systole where this pressure wave is important. During diastole though, this assumption of infinite pressure wave velocity is less influential on the results since the pressure is constant throughout the systemic system and yields more realistic predictions (Aperia, 1940). This assumption explains why the windkessel model produces more accurate results for high pressure wave cases, e.g. more rigid arteries from increasing age, arteriosclerosis, or vasoconstriction (Skalak, 1972).

Before Hales discoveries, mathematical equations were being derived to explain the basic principles of general fluid mechanics. Two of the first fundamental laws were Newton's conservation of mass and momentum. Based on these laws, the mathematical theories to model segmental flow were derived, many of which have become the foundation of modern fluid dynamics. Applying the physical principle of the conservation of mass to a finite control volume fixed in space leads to the *continuity equation*, which states that the rate at which the fluid mass within an arbitrary volume is changing must be equal to the rate at which the mass is flowing from the volume:

$$-\frac{\partial}{\partial t}\int_V \rho dV = \int_S \rho \mathbf{n}\cdot\mathbf{q}dS \tag{2.2}$$

Newton's second law of momentum conservation states that the rate of change of linear momentum of a mass of fluid must balance the resultant force acting on the mass:

$$\mathbf{F} = \int_S \rho\mathbf{q}(\mathbf{n}\cdot\mathbf{q})dS + \int_V \frac{\partial\rho\mathbf{q}}{\partial t}dV \tag{2.3}$$

where $\mathbf{F}$ is the resultant force on the control volume, and $\rho\mathbf{q}$ is the linear momentum per unit volume. From Newton's second law, the *Navier-Stokes* equations were derived which describe general fluid motion for incompressible, constant viscosity fluids:

$$\frac{\partial\mathbf{q}}{\partial t} + (\mathbf{q}\cdot\nabla)\mathbf{q} = -\frac{1}{\rho}\nabla p + \mathbf{B} + \frac{\mu}{\rho}\nabla^2\mathbf{q} \tag{2.4}$$

where $\frac{\partial\mathbf{q}}{\partial t}$ is the local acceleration (equal to zero for steady flow), $(\mathbf{q}\cdot\nabla)\mathbf{q}$ is the convective acceleration, and $\mathbf{B}$ represents the body force. These nonlinear partial differential equations are the governing equations for viscous fluids and are used as the starting point in the analysis of many fluid mechanics problems. These will be examined next.

Extended Mathematical Applied Theories Various researchers of the twentieth century (Witzig, 1914; Aperia, 1940; Morgan and Kiely, 1954; Womersley, 1955a; Uchida, 1956; McDonald, 1974) used certain simplifying assumptions that enabled them to obtain analytic solutions for reduced forms of the Navier-Stokes equations. Womersley published a series of technical reports on linearized theories of pulsatile flow between 1955 to 1957. In his first report (1955a,b), Womersley developed an analytical solution to oscillatory flow through straight, circular rigid tubes by linearization of the Navier-Stokes equation. By using the superposition principle which applies to linear systems, he was able to provide solutions for harmonic os-

cillations only. The complicated flow waveforms are broken down into their Fourier components and the solutions to each can be added for the complete solution. In 1957, he included the effects of wall elasticity in his solution, as well as proposing a vascular tethering model to represent the reaction of the surrounding tissue to the motion of the arterial wall. The linear theories that Womersley developed are useful for describing certain aspects of flow in relatively rigid arteries, but they still failed to give a complete representation of the flow field in arteries.

Another approach to arterial flow modeling is the one-dimensional flow model. Fox and Saible (1965) integrated the continuity and momentum equations over the cross section of a circular tube to yield:

$$\frac{\partial A}{\partial t} + \frac{\partial Q}{\partial x} + \psi = 0 \tag{2.5}$$

$$\frac{\partial Q}{\partial t} + \frac{\partial}{\partial x}\int u^2 dA = -\frac{A}{\rho}\frac{\partial p}{\partial x} + \frac{2\pi R\tau_\omega}{\rho} + Ab_x \tag{2.6}$$

where u is the velocity in the longitudinal direction, A is the cross sectional area, p is the arterial pressure, Q is the flow rate, b_x is the body force vector component in the axial direction, ψ represents seepage through the walls of small branches per unit length, and τ_w is the shear stress on the inner wall. In the same line of thought, the following assumptions were made by several authors (Young, 1979; Rooz et al., 1982; Porenta et al., 1986; Weerappuli, 1987; Balar et al, 1989; Stergiopulos et al., 1992) in developing the governing equations for an arterial model:

- An artery can be considered a linearly varying tapered tube of circular cross section.

- The walls of the artery can be considered elastic, thin, and incompressible with properties that are constant throughout the segment length.

- The artery is constrained in the longitudinal direction.
- Blood is treated as an incompressible, homogeneous, isotropic, Newtonian fluid.
- Pressure does not vary along the radius.
- Flow is laminar and axisymmetric except at localized constrictions; there are no secondary flows.

Though these assumptions do not strictly hold for several cases of arterial flow, they prove a reasonable estimation to the conservation equations. Integrating the momentum and continuity equations over the cross-section of an artery using the above assumptions and neglecting seepage, the one-dimensional flow equations for continuity and momentum are, respectively

$$\frac{\partial A}{\partial t} + \frac{\partial Q}{\partial x} = 0 \tag{2.7}$$

$$\frac{\partial Q}{\partial t} + \frac{\partial}{\partial x}\left(\frac{Q^2}{A}\right) = -\frac{A}{\rho}\frac{\partial p}{\partial x} + \frac{\pi D \tau_w}{\rho} \tag{2.8}$$

where $\left(\frac{Q^2}{A}\right)$ is the convective acceleration term. The shear stress is an unknown quantity and needs to be evaluated. To do this a knowledge of the flow velocity profile in the vicinity of the wall needs to be found. An approximation method used in the past for the shear stress assumes that the velocity profile is parabolic at all times (Poiseuille's Law), so that:

$$\tau_w = -\frac{4\mu}{\pi R^3} Q \tag{2.9}$$

(Raines et al., 1974; Rockwell et al., 1974; Rumberger and Nerem, 1977; Rooz, 1980; Young et al., 1980; Porenta, 1982; Rangarajan, 1983; Porenta et al., 1986). However,

experimental measurements show that the velocity profile is rather blunt with steep gradients existing near the wall, especially in larger arteries (Ling et al., 1968; McDonald, 1974). In fact, McDonald (1974) suggested that there was an approximate 50% increase in flow resistance as compared to steady flow at the wall due to the induced steeper gradients from oscillatory flow. Raines et al. (1974) compensated for that by increasing the blood viscosity value by 10% in their calculations.

Schaaf and Abbrecht (1972) attempted to improve the wall stress approximation using a formula derived from a model of pulsatile flow in a rigid, infinite, cylindrical tube:

$$\tau_w = \frac{8\mu}{D}U + \frac{\rho D(\lambda - 1)}{4}\frac{\partial U}{\partial t} \tag{2.10}$$

where $U = Q/A$ is the instantaneous cross sectional average velocity and λ is the momentum flux coefficient defined as

$$\lambda = \frac{1}{A}\int \frac{u^2}{U^2} dA \tag{2.11}$$

For a parabolic velocity profile, $\lambda = \frac{4}{3}$ was calculated. If $\lambda = 1$ is used, the unsteady term would drop off and Eq. 2.10 will look similar to Eq. 2.9, yielding similar results. Also, when all frictional effects were removed by setting viscosity to zero, there was a negligible difference in shear stress results, thus concluding that wall shear stress plays a very small role in pulse formation in the arterial system.

Concurrently in 1972, Wemple and Mockros derived a shear stress model based on Womersley's solution that took into account the unsteady flow oscillation components in a straight, rigid tube:

$$\tau_w = \pi\mu\alpha^2 \frac{sin\epsilon_{10}}{AM_{10}}Q + \frac{\pi\mu\alpha^2}{A\omega}\left(\frac{cos\epsilon_{10}}{M_{10}} - 1\right)\frac{\partial Q}{\partial t} \tag{2.12}$$

where

$$M_{10}e^{i\epsilon_{10}} = 1 - \frac{2J_1(\alpha i^{\frac{3}{2}})}{\alpha i^{\frac{3}{2}} J_0(\alpha i^{\frac{3}{2}})} \tag{2.13}$$

$J_0(\alpha i^{\frac{3}{2}})$ and $J_1(\alpha i^{\frac{3}{2}})$ are Bessel functions of the first kind of order zero and one, respectively. The values for M_{10} and ϵ_{10} are tabulated in McDonald (1974) as functions of the α parameter. The α parameter, sometimes called the Womersley or frequency parameter, is one of the governing parameters for oscillating flow and can be defined as $\alpha = R\sqrt{\frac{\omega}{\nu}}$, where R is the vessel radius, ω is the angular frequency (rad/sec), and ν is the kinematic viscosity of the fluid. If $\alpha \gg 1$, then flow is highly pulsatile and inertial forces are predominant. If $\alpha < 1$, then the flow is quasi-steady, meaning the viscous forces dominate and the inertial forces can be neglected. The α values in human arteries usually range from 1 (small arteries) to 17 (aorta). After comparing results using Eq. 2.12 with the results of the shear stress set to zero, Wemple and Mockros came to the same conclusion as Schaaf and Abbrecht did that wall shear stress is negligible in the arteries. A little later, Young and Tsai (1973b) arrived at a shear stress relation based on Womersley's solution to oscillatory flow that was similar to Eq. 2.12:

$$\tau_w = -\frac{\rho}{2\pi R}\left[\frac{8c_v\pi\mu}{\rho A}Q + (c_u - 1)\frac{\partial Q}{\partial t}\right] \tag{2.14}$$

The semi-empirical coefficients c_v and c_u represent the semi-empirical coefficients of the viscous and unsteady term and are a function of the α parameter,thus, they can be evaluated only for the case of purely harmonic flow. These coefficients can be calculated from Young's exact solution of

$$\Delta p = c_v\left(\frac{32\mu L}{D^2}\right)U + c_u\rho L\frac{dU}{dt} \tag{2.15}$$

where D is the tube diameter and U is the average instantaneous velocity. Figure 2.1 shows the c_v and c_u values found by Young and Tsai for α parameters up to 20.

In addition to Eqs. 2.7 and 2.8, an equation describing the distensibility of the arterial wall as a function of a change in pressure must be specified. The simplest form of pressure-area relation used by several past researchers (Snyder et al., 1968; Westerhof et al., 1969; Young et al., 1980) is a linearly varying relationship based on the assumption that a linear curve can produce relatively accurate approximations within the operational range of distending pressures. This linear relationship is described as

$$A(p,x) = A_o(x) + C(x)(p - p_o) \tag{2.16}$$

where A_o is the cross sectional area at reference pressure p_o, and C is the compliance. Overall, the above linear arterial pressure-area relation was proved to be incorrect from experimental studies in humans and canines (Bergel, 1961; Mozersky et al., 1972; Anliker et al., 1978;) so nonlinear forms of the pressure-area relationship need to be examined.

Streeter et al. (1963) derived the theoretical expression

$$A(p,x) = A_o(x)\left[1 - \frac{D_o(p - p_o)}{h_o E}\right]^{-1} \tag{2.17}$$

based on the consideration that the artery is a thin-walled, incompressible, elastic vessel. D_o and h_o are the arterial diameter and wall thickness, respectively, at the reference pressure p_o, and E is the elastic modulus.

Wemple and Mockros (1972) introduced an exponential relationship between the radius and elastic modulus which resulted in the equation

$$\frac{p}{2a_o^2} = \frac{R_o}{R}\left[\frac{1}{\beta}\left[\left(\frac{R}{R_o}\right)^{\beta} - 1\right] + \frac{p_o}{2a_o^2}\right] \tag{2.18}$$

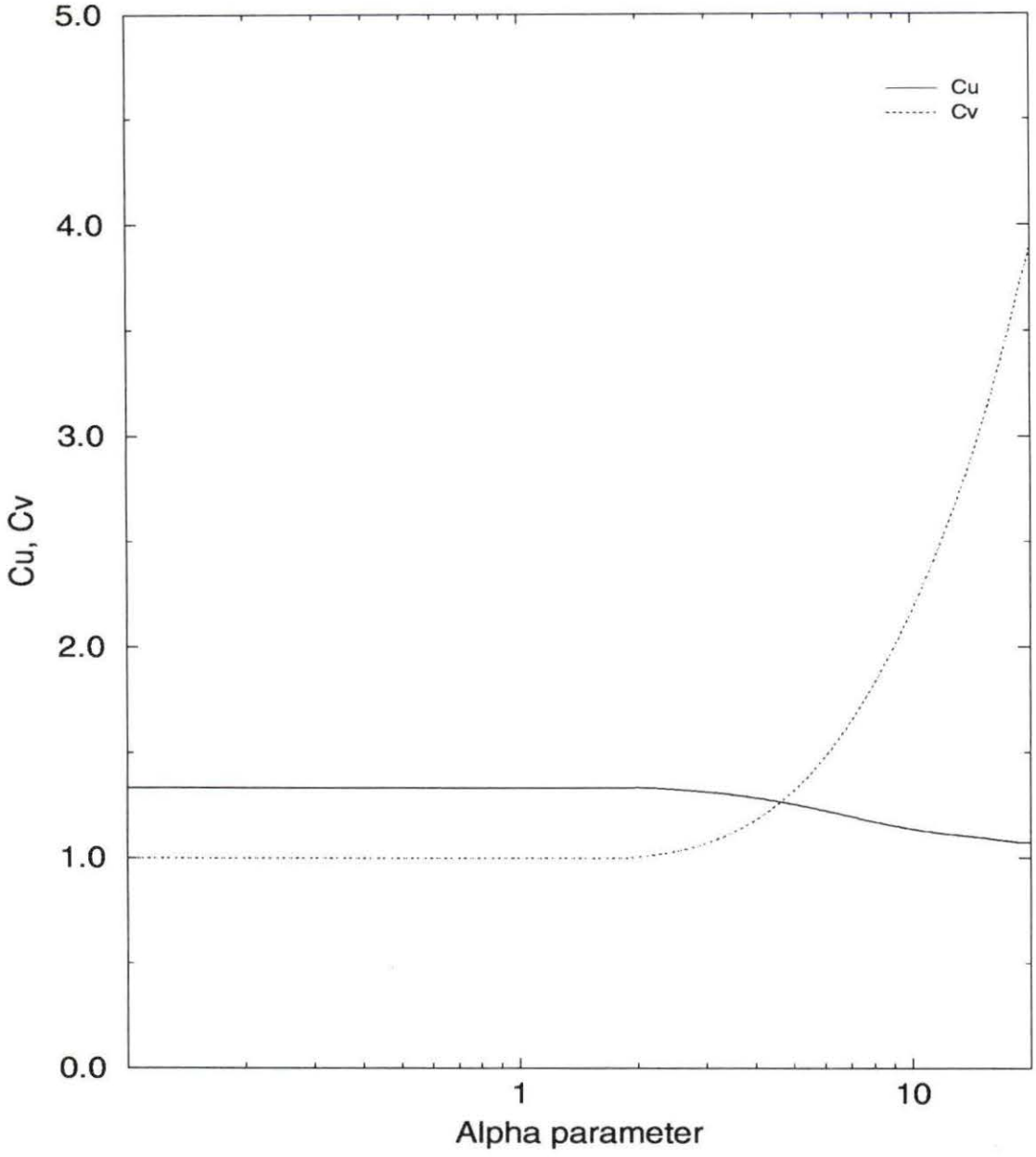

Figure 2.1: Coefficients of wall shearing stress for simple harmonic flow in a straight, rigid tube (Young and Tsai, 1973b)

where β is an experimentally derived constant and a_o is the velocity of the local wave. Rumberger and Nerem (1977) suggested another exponential form of the pressure-area relation:

$$A(p,x) = A_o(x)e^{\frac{p-p_o}{\rho c(p,x)c_o(p_o,x)}} \tag{2.19}$$

where c and c_o are the wave propagation velocities at the distending pressure p and reference pressure p_o, respectively. This pressure-area relationship has the advantage of relying on the more easily obtainable wave velocities c and c_o than on other compliance related quantities, such as wall thickness and modulus of elasticity.

Another way to express the equation of state was suggested by Raines et al. (1974). They proposed that there is an inverse relationship between compliance and pressure, and with that in mind the following logorithimic pressure-area relationship was arrived at:

$$A(p,x) = A_o(p_o,x) + \beta ln\frac{p}{p_o} \tag{2.20}$$

where β is an empirical quantity related to the artery's elastic properties. A quadratic expression for the equation of state was formulated by Rooz (1980), but not via theoretical analysis. Instead, this quadratic form was a convenient extension of the linear constitutive relation mentioned earlier (Eq. 2.16) and is capable of accounting for the nonlinear properties of the arterial wall. The equation is:

$$A(x) = A_o(x) + C_o(p-p_o) + C_1(p-p_o)^2 \tag{2.21}$$

This form has been used by several researchers (Rooz et al., 1982; Porenta, 1982; Porenta et al., 1986; Weerappuli, 1987; Balar et al.,1989; Stergiopulos et al., 1992) in their governing equations. This relation yields a linear dependence of the area compliance, $C = dA/dp$, on pressure. Stergiopulos et al. (1994) proposed an area

compliance-pressure relation based on the work of Langewouters et al. (1984) that accounted for the strong nonlinear dependence of compliance on pressure that could be applied easily to all arterial segments with a small percentage of error in model overestimation. This compliance-pressure relationship, which will be employed in this research, is of the following form:

$$C_a = C_{ref}\left(\frac{a+b}{\left(1+\frac{P-P_a}{P_b}\right)^2}\right) \tag{2.22}$$

where C_{ref} is the area compliance of the segment at the reference pressure of 100 mmHg, P is pressure, $P_a = 20mmHg$, $P_b = 30mmHg$, and a, b are empirical constants experimentally determined to be 0.4 and 5, respectively. Assuming that arterial compliance is given as $C_a = \frac{\partial A}{\partial p}$, Eq. 2.7 can be rewritten as:

$$\frac{\partial Q}{\partial x} + C_a\frac{\partial p}{\partial t} = 0 \tag{2.23}$$

Substituting the wall shear stress expression of Eq. 2.14 into Eq. 2.8 yields:

$$c_u\frac{\partial Q}{\partial t} + \frac{\partial}{\partial x}\left(\frac{Q^2}{A}\right) + \frac{A}{\rho}\frac{\partial p}{\partial x} + B_1 Q = 0 \tag{2.24}$$

where $B_1 = (8c_v\pi\mu)/(\rho A)$. The area, $A(x,t)$, is given an initial value along the arterial segment so that the variables $p(x,t)$ and $Q(x,t)$ can be solved given the initial boundary conditions.

Arterial Stenosis Models As mentioned before, a stenosis is the localized narrowing of a vessel caused by plaque buildup. A general experimental and theoretical simulation used for arterial stenosis is a Venturi or convergent-divergent duct similar to that used in low-speed windtunnels, where pressure drops and velocity increases at the constriction. If the stenosis is severe enough, the excessive

resistance will cause the mean flow to drop so that there is inadequate perfusion of blood to the distal beds and the tissue will die. Hence an equation to model the pressure drop across the stenosis needs to include the flow characteristics of viscous effects, turbulence, and the inertia effects from unsteady flow. Since stenosis models are extremely difficult to compose numerically or analytically due to their complex geometry induced non-linearities and the presence of turbulence, the models have mostly been determined experimentally. Young and Tsai (1973a,b) approximated an induced pressure drop, $\Delta p(t)$, through axisymmetric and nonsymmetric stenoses from in vitro experimental studies on steady and pulsatile flow using the following equation:

$$\Delta p(t) = \frac{K_v \mu}{D} U(t) + \frac{K_t \rho}{2} \left[\frac{A_o}{A_s} - 1 \right]^2 \mid U(t) \mid U(t) + K_u \rho L_s \frac{dU(t)}{dt} \qquad (2.25)$$

where

A_o = unconstricted cross sectional lumen area

A_s = minimum cross sectional lumen area inside the constricted area

D = diameter of the unobstructed tube

K_t = empirical coefficient of the turbulence term

K_u = empirical coefficient of the unsteady term

K_v = empirical coefficient of the viscous term

L_s = length of the stenosis

U = instantaneous cross sectional average velocity in unconstricted area

On the right hand side of Eq. 2.25, the first term represents the pressure change due to viscous effects, the second term represents the turbulence and accounts for nonlinear losses, and the final term represents the inertia effects from the unsteady flow.

Later, Young et al. (1975) performed in vivo experiments on dogs to test the relevancy of this stenosis model. Rigid, hollow, cylindrical plugs were placed in the femoral arteries of the dogs to simulate a stenosis. The blood flow and pressure drop were measured across the artificial constriction of the artery and compared to results calculated from Eq. 2.25. These measurements confirmed that the stenosis model yielded satisfactory results. The effect of stenosis geometry on pressure losses across models of arterial stenoses was examined more carefully in 1976 by Seeley and Young. They found that the coefficients K_u and K_t were dependent slightly on geometry while the coefficient K_v was strongly dependent on the geometry. For the blunt-ended stenoses used in the study, K_u and K_t can be approximated to be 1.2 and 1.52, respectively, while K_v was statistically determined as being the following relation:

$$K_v = 32\frac{0.83L_s + 1.64D_s}{D}\left(\frac{A_o}{A_1}\right)^2 \tag{2.26}$$

where A_1 is the minimum cross-sectional area of stenosis and D_s is the diameter corresponding to area A_s. Young (1979) presents a full review of the fluid mechanics of arterial stenosis.

Computational Fluid Dynamic Models of Circulation Computers have aided the hemodynamicists by allowing them to use numerical techniques on nonlinear and linear systems to obtain solutions. The method of characteristics (Anliker et al., 1971; Wemple and Mockros, 1972; Schaaf and Abbrecht, 1972), finite element method (Rooz et al., 1982; Porenta et al., 1986; Weerappuli, 1987; Balar et al., 1989; Stergiopulos et al., 1992), and finite difference method (Raines et al., 1974; Stergiopulos, 1992) have been popular numerical methods used in computational

fluid dynamic problem solving. Raines et al. (1974) opted for the finite difference method over the method of characteristics in their nonlinear computational model of the human leg because it was more convenient and economical. For both normal and various diseased arterial flow cases, the computational results proved to be in relatively good agreement with experimental results. Rooz et al. (1982) employed the Galerkin method to develop a finite element model to obtain their solution. It uses linear isoparametric quadrilateral elements to transform the partial differential equation system into a set of algebraic equations.

Porenta et al. (1986) applied the Galerkin method to the Raines et al. (1974) leg model, but they discretized the equations only in space to arrive at a system of ordinary differential equations (ODE) which they solved using a difference method. Weerappuli (1987), Balar et al. (1989), and Stergiopulos et al. (1992) all followed Porenta's approach but each studied a different aspect of arterial flow. Weerappuli studied the uterine artery of the cow and the femoral artery of a dog, Balar studied the arteries of the human arm, and Stergiopulos modeled the major arteries of the entire human body. Both Weerappuli and Stergiopulos found that the finite difference method was a more stable method to use for the systemic circulation model.

The finite difference scheme utilized by Stergiopulos et al. (1992) to model the entire systemic circulatory system will be incorporated in this study. An expanded discussion of the governing equations, boundary conditions, and finite difference method used here can be found in their paper on computer simulation of arterial blood flow.

CHAPTER 3. MODEL EQUATIONS, BOUNDARY CONDITIONS, AND ARTERIAL GEOMETRY

Governing Equations

The non-linear computer model around which this study is based was developed by Nikolaos Stergiopulos et al. (1992). All assumptions and a complete derivation of the governing equations and boundary conditions can be found in this work and earlier works presented by Porenta et al. (1986), Weerappuli (1987), Balar et al. (1989), Rooz et al. (1982), and Young (1979). The model utilizes the finite difference method to solve the model equations of the systemic arterial system based on the one-dimensional flow equations (Eqs. 2.23 and 2.24). The program also incorporates an area compliance-pressure relationship (Eq. 2.22) that accounts for the the non-linear dependence of compliance on pressure (Stergiopulos et al., 1994) and calculates the wall shearing stress constants for simple harmonic flow (Eq. 2.14) as predicted by Young and Tsai (1973b). For the special case of a stenosis, the pressure drop can be empirically predicted by Eq. 2.25 from the instantaneous flow through the stenosis (Young and Tsai, 1973b). Vasodilation is accounted for after a stenosis by reducing the peripheral resistances so that the mean flow stays constant until maximum vasodilation is reached. There is a corresponding critical stenosis severity point beyond which the peripheral beds cannot dilate and any increase in stenosis

severity would result in a reduction of mean flow. Thus, the critical stenosis value is a function of stenosis location as well as the degree of maximum distal vasodilation. The following sections contain the boundary conditions as well as the initial geometrical data.

Boundary Conditions

The proximal boundary condition is a pressure input waveform originating at the root of the ascending aorta. This waveform is approximated by Fourier coefficients as shown in Table 3.1 for a heart rate of 78 bpm (adapted from Balar et al., 1989). The coefficients have been adjusted so that the waveform has a frequency of 1.0 Hz to add stability to the computer model which did not respond well to frequencies over 1.0. The adjusted Fourier coefficients for conditions of hypertension, valvular aortic stenosis (AS), aortic regurgitation (AI), and a combination of aortic stenosis and regurgitation (AS/AI) are presented in Tables 3.2, 3.3, 3.4, and 3.5, respectively.

Table 3.1: Fourier coefficients for the control proximal pressure waveform

Harmonics	Cosine coefficients (N/m^2)	Sine coefficients (N/m^2)
0	$0.10429E+5$	$0.00000E+0$
1	$-0.42968E+2$	$0.20234E+4$
2	$-0.11870E+4$	$0.12991E+4$
3	$-0.54298E+3$	$0.10251E+3$
4	$-0.51053E+3$	$-0.87610E+2$
5	$-0.22631E+3$	$-0.21803E+3$
6	$-0.14697E+2$	$-0.13085E+3$

Table 3.2: Fourier coefficients for the hypertensive proximal pressure waveform

Harmonics	Cosine coefficients (N/m^2)	Sine coefficients (N/m^2)
0	$0.18046E+5$	$0.00000E+0$
1	$-0.24396E+4$	$0.31741E+4$
2	$-0.18267E+4$	$-0.65979E+3$
3	$-0.75191E+2$	$-0.76335E+3$
4	$0.14851E+3$	$-0.17980E+3$
5	$0.28175E+2$	$-0.27715E+2$
6	$-0.16979E+2$	$-0.52930E+1$

Table 3.3: Fourier coefficients for the AS proximal pressure waveform

Harmonics	Cosine coefficients (N/m^2)	Sine coefficients (N/m^2)
0	$0.92645E+4$	$0.00000E+0$
1	$-0.12679E+4$	$0.17046E+4$
2	$-0.88559E+3$	$-0.24220E+3$
3	$0.96316E+2$	$-0.15932E+3$
4	$-0.11488E+3$	$0.13633E+2$
5	$-0.35201E+2$	$-0.23423E+2$
6	$-0.80068E+1$	$0.17898E+2$

Pressure is assumed constant and flow continuity is preserved at bifurcations throughout the arterial system. For the distal boundary conditions, a lumped parameter impedance model is used for each terminal branch to account for the capacitances and resistances of microvasculature at the distal end of the terminal branch. The model used is the modified windkessel model which relates pressure and flow by placing a parallel combination of a resistance and a capacitance in series with a

Table 3.4: Fourier coefficients for the AI proximal pressure waveform

Harmonics	Cosine coefficients (N/m^2)	Sine coefficients (N/m^2)
0	$0.10803E+5$	$0.00000E+0$
1	$-0.20556E+3$	$0.31809E+4$
2	$-0.16733E+4$	$0.38094E+3$
3	$-0.10787E+4$	$-0.39764E+2$
4	$-0.36991E+3$	$-0.38443E+3$
5	$-0.18153E+3$	$-0.32758E+3$
6	$-0.37397E+2$	$-0.18144E+3$

Table 3.5: Fourier coefficients for the AS/AI proximal pressure waveform

Harmonics	Cosine coefficients (N/m^2)	Sine coefficients (N/m^2)
0	$0.14770E+5$	$0.00000E+0$
1	$-0.61254E+4$	$0.28294E+4$
2	$0.23338E+3$	$-0.17480E+4$
3	$-0.27714E+3$	$0.97066E+3$
4	$-0.73641E+3$	$-0.43141E+3$
5	$-0.12954E+3$	$-0.60237E+3$
6	$-0.18964E+1$	$-0.23880E+3$

second resistance to simulate the compliance of the terminal beds:

$$\frac{dQ}{dt} = \frac{1}{R_1}\frac{dp}{dt} + \frac{p}{R_1 R_2 C_T} - \left(1 + \frac{R_1}{R_2}\right)\frac{Q}{R_1 C_T} \tag{3.1}$$

Total peripheral resistance for any terminal branch is $R_1 + R_2 = R_T$. In the special case where $C_T = 0$ the modified windkessel model degenerates to a simple resistance and Eq. 3.1 becomes $Q = \frac{p}{R_T}$.

Physiological Data

The physiological model of the human arterial tree consists of 55 segments (Fig. 3.1) that cover most of the major arteries of a healthy young adult. Those arteries not covered include the coronary arteries and the vasculature of the hands, feet, thoracic cavity, abdominal cavity, and cranium. The geometrical data shown in Table 3.6 is considered the control case data and includes the segment length, entry and exit radii, orientation, and volume compliance. Table 3.7 shows terminal impedance data. Both tables are supplied by Stergiopulos et al. (1992). The body model is represented in a supine or standing position with all limbs straight and hands suponated. Appendices A and B are sample input files for the computational model for a normal flow case and for a 90% stenosis case in the left femoral artery.

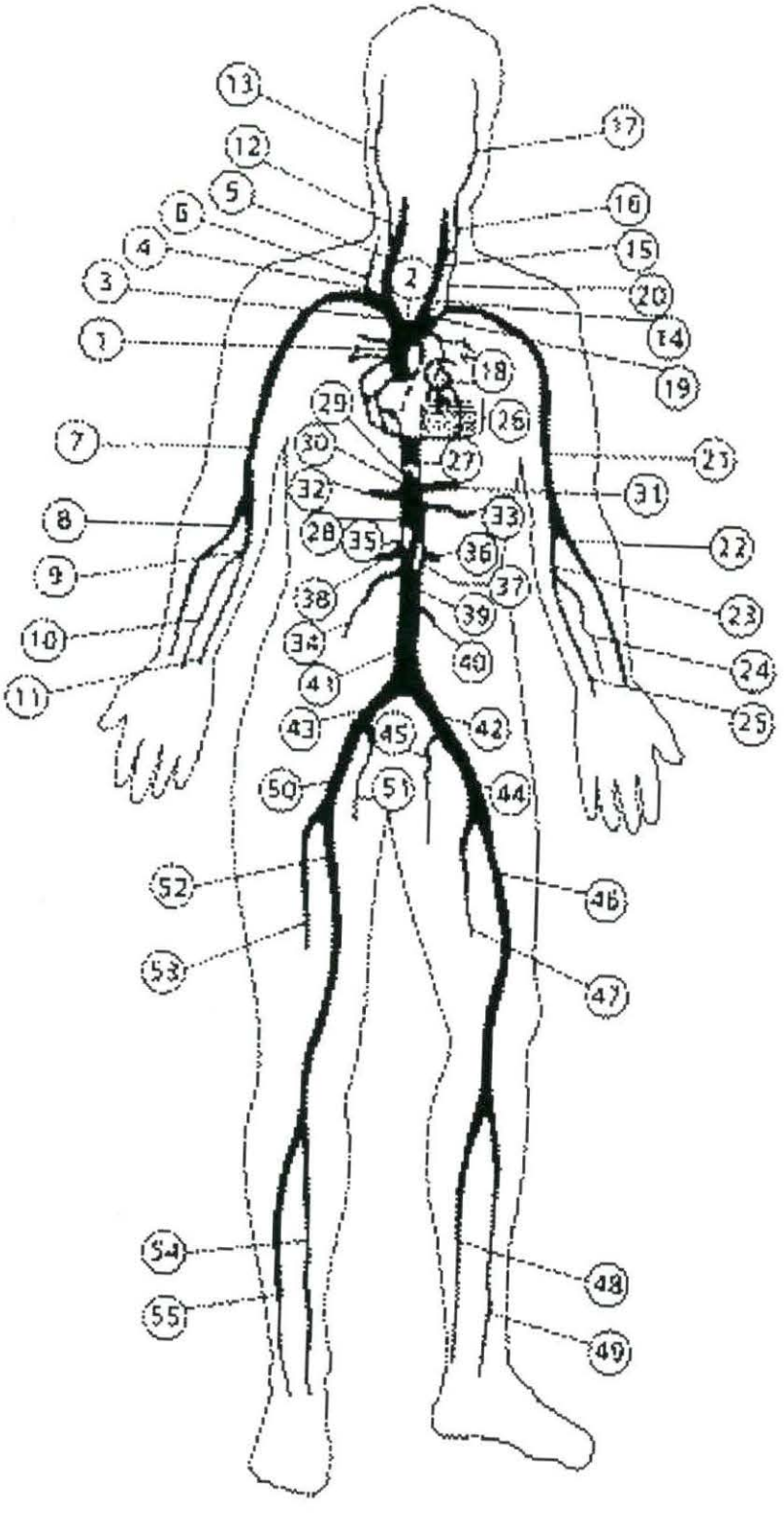

Figure 3.1: Geometric model

Table 3.6: Arterial geometric data (Stergiopulos et al., 1992)

Seg	Name	Length (cm)	Prox. R (cm)	Distal R (cm)	Angle (deg)	Vol. compl. ($10^{-6}\frac{cm^5}{dyne}$)
1	Ascending Aorta	4.0	1.470	1.440	90	104.400
2	Aortic Arch	2.0	1.120	1.120	0	29.600
3	Innominate	3.4	0.620	0.620	135	13.500
4	R. Subclavian A	3.4	0.423	0.423	180	5.600
5	R. Carotid	17.7	0.370	0.370	90	21.360
6	R. Vertebral	14.8	0.188	0.183	120	1.682
7	R. Subclavian B	42.2	0.403	0.236	240	33.870
8	R. Radial	23.5	0.174	0.142	240	1.877
9	R. Ulnar A	6.7	0.215	0.215	240	1.110
10	R. Interosseous	7.9	0.091	0.091	240	0.090
11	R. Ulnar B	17.1	0.203	0.183	240	2.210
12	R. Internal Carotid	17.7	0.177	0.083	90	0.943
13	R. External Carotid	17.7	0.177	0.083	135	0.943
14	Aortic Arch B	3.9	1.070	1.070	0	52.100
15	L. Carotid	20.8	0.370	0.370	60	25.100
16	L. Internal Carotid	17.7	0.177	0.083	90	0.943
17	L. External Carotid	17.7	0.177	0.083	45	0.943
18	Thoracic Aorta A	5.2	0.999	0.999	270	59.700
19	L. Subclavian A	3.4	0.423	0.423	45	5.600
20	Vertebral	14.8	0.188	0.183	60	1.682
21	L. Subclavian B	42.2	0.403	0.236	300	33.870
22	L. Radial	23.5	0.174	0.142	300	1.877
23	L. Ulnar A	6.7	0.215	0.215	300	1.110
24	L. Interosseous	7.9	0.091	0.091	300	0.090
25	L. Ulnar B	17.1	0.203	0.183	300	2.210
26	Intercostals	8.0	0.200	0.150	0	3.000
27	Thoracic Aorta B	10.4	0.675	0.645	270	47.600
28	Abdominal Aorta A	5.3	0.610	0.610	270	20.400
29	Celiac A	1.0	0.390	0.390	0	1.360
30	Celiac B	1.0	0.200	0.200	0	1.000
31	Hepatic	6.6	0.220	0.220	315	2.300
32	Gastric	7.1	0.180	0.180	450	1.510
33	Splenic	6.3	0.275	0.275	0	3.740
34	Superior Mesenteric	5.9	0.435	0.435	225	10.400
35	Abdominal Aorta B	1.0	0.600	0.600	270	4.000
36	L. Renal	3.2	0.260	0.260	0	1.670
37	Abdominal Aorta C	1.0	0.590	0.590	270	3.800

Table 3.6 (Continued)

Seg	Name	Length (cm)	Prox. R (cm)	Dist. R (cm)	Angle (deg)	Vol. compl. ($10^{-6}\frac{cm^5}{dyne}$)
38	R. Renal	3.2	0.260	0.260	0	1.670
39	Abdominal Aorta D	10.6	0.580	0.548	270	33.900
40	Inferior Mesenteric	5.0	0.160	0.160	270	0.792
41	Abdominal Aorta E	1.0	0.520	0.520	270	3.500
42	L. Common Iliac	5.8	0.368	0.350	315	4.580
43	R. Common Iliac	5.8	0.368	0.350	315	4.580
44	L. External Iliac	14.4	0.320	0.270	315	15.620
45	L. Internal Iliac	5.0	0.200	0.200	270	3.300
46	L. Femoral	44.3	0.259	0.190	270	13.640
47	L. Deep Femoral	12.6	0.255	0.186	315	1.130
48	L. Posterior Tibial	32.1	0.247	0.141	270	2.206
49	L. Anterior Tibial	34.3	0.130	0.130	270	0.842
50	R. External Iliac	14.4	0.320	0.270	225	15.620
51	R. Internal Iliac	5.0	0.200	0.200	270	3.300
52	R. Femoral	44.3	0.259	0.190	270	13.640
53	R. Deep Femoral	12.6	0.255	0.186	225	1.130
54	R. Posterior Tibial	32.1	0.247	0.141	270	2.206
55	R. Anterior Tibial	34.3	0.130	0.130	270	0.842

Table 3.7: Terminal impedance data (Stergiopulos et al., 1992)

Seg	Total Resistance $(\frac{N \cdot s}{m^5})$	Terminal Compliance $(\frac{m^5}{N})$
6	0.60100E+10	0.30955E-10
8	0.52800E+10	0.35235E-10
10	0.84300E+11	0.22069E-11
11	0.52800E+10	0.35235E-10
12	0.13900E+11	0.13384E-10
13	0.13900E+11	0.13384E-10
16	0.13900E+11	0.13384E-10
17	0.13900E+11	0.13384E-10
20	0.60100E+10	0.30955E-10
22	0.52800E+10	0.35235E-10
24	0.84300E+11	0.22069E-11
25	0.52800E+10	0.35235E-10
26	0.13900E+10	0.13384E-09
31	0.36300E+10	0.51251E-10
32	0.54100E+10	0.34389E-10
33	0.23200E+10	0.80191E-10
34	0.93000E+09	0.20005E-09
36	0.11300E+10	0.16464E-09
38	0.11300E+10	0.16464E-09
40	0.68800E+10	0.27041E-10
45	0.79360E+10	0.23443E-10
47	0.47700E+10	0.39003E-10
48	0.47700E+10	0.39003E-10
49	0.55900E+10	0.33281E-10
51	0.79360E+10	0.23443E-10
53	0.47700E+10	0.39003E-10
54	0.47700E+10	0.39003E-10
55	0.55900E+10	0.33281E-10

CHAPTER 4. MODIFICATIONS AND INDICES

In this chapter, the modifications to the computational full body arterial finite difference model and what will be accomplished specifically for this thesis will be discussed. The focus of this research will be to (1) increase the output information of the model to make it more descriptive as well as more versatile, (2) incorporate indices into the model, and (3) study influences of various flow disfunctions at various points in the arterial tree on these indices in terms of their sensitivity as well as their ability to predict a stenosis.

Program Versatility

The original program uses a predetermined input file and asks for two nodes for which waveforms can be plotted as the only options. The output data produced is (1) verification of the input data (including the node numbers assigned to each arterial segment, X and Y nodal coordinates, and initial pressure and flow values for each node), (2) minimum, maximum, and average pressure and flow values for all nodes of the model, (3) pressure and flow waveform data for the two specified nodes, and (4) area versus pressure data for the two specified nodes to demonstrate the compliance of the vessel at those nodes during systole and diastole. To increase the programs capabilities, for possible use in a clinical environment, additional command options

are issued that make the user more aware of what is available as well as giving broader choices for output.

First, rather than limiting the user to two nodes in the body for which flow and pressure waveforms will be plotted, up to ten nodes per input file may be chosen for their waveform information. At completion of solving the pressure and flow equations, the user is allowed the option of calculating indices for the selected nodes. Also, any number of arterial segments may be chosen for their flow velocity and pressure profiles as well as index and information so that an entire segment may be studied at once. Choosing specific segments for the minimum, maximum, and average pressure and flow data is more advantageous than examining data of the entire body. The indices calculated from the user specified nodes can be normalized for easier comparison to the control case. All the pressure and flow information is already calculated in the program so it is only a matter of manipulating the program to output the data to a graphical file.

In an effort to make the program more physiologically realistic, a new compliance relation is incorporated into the model as well as calculating new wall shear coefficients, c_u and c_v, at every node throughout the arterial tree. Vasodilation can be accounted for in the stenosis cases by entering whether there are terminal segments below the stenosis that must have their total terminal resistance reduced so that the mean flow stays constant. It is assumed that vasodilation will decrease the terminal impedance up to 20% of the original impedance (Manor et al., 1994).

Flow Waveform Indices

Non-invasive diagnostic methods for the assessment of abnormal arterial flow have been a preferred alternative to invasive techniques due to reduced risk and expense. Ultrasonic devices have been the most frequently used non-invasive diagnostic tool in a clinical environment since they can be used quickly and safely on a regular basis for routine screening of arteries close to the surface of the skin. Such arteries include the carotid arteries in the neck, the brachial, radial, and ulnar arteries in the arm, and the femoral, popliteal, tibial and dorsalis pedis arteries in the leg and foot. The use of Doppler ultrasound along with the facilitation of calculated dimensionless indices can be very instrumental in detecting an arterial stenosis and is the method that will be discussed in depth here.

There are several types of ultrasonic flow meters and techniques used to determined peripheral arterial blood flow at a specific point. A Doppler flow meter can display all frequencies occurring in the Doppler signal versus time. Two specific Doppler flow meters of note are the *pulsed Doppler flow meter* and the *continuous wave Doppler flow meter*. The pulsed Doppler flow meter produce audio signals for a restricted area of the total arterial lumen while the continuous wave Doppler flow meter determines an average velocity over the total arterial cross section. In general, for laminar blood flow, the Doppler energy is concentrated in a narrow frequency band, whereas for turbulent flow indicating a possible stenosis, the energy is spread over a wider frequency range. Each artery has a unique audio signal and velocity waveform characteristic which the Doppler flow meter can detect. An experienced clinician can distinguish if the artery is normal or abnormal from these audio signals and waveform recordings. In order to decrease subjectivity of interpretation, wave-

form indices have been developed to accompany the energy frequency spectrum data to make comparisons between velocity waveforms easier.

Various indices have been developed by researchers which are useful for different arteries. The measurement and calculation of indices from chart recordings is rather tedious and is the main reason why they have not gained world wide acceptance. With the advent of computers, calculation of indices has become relatively simple and instantaneous. One of the most commonly known and used indices is the *pulsatility index*. In 1971, Gosling et al. defined the pulsatility index (PI) as the total oscillatory energy in the flow velocity divided by the energy of the mean forward flow velocity during a cardiac cycle. Gosling could arrive at a quantitative comparison of the arterial pathway capabilities of different patients by looking at the variation of the PI from the abdominal aorta to the tibial arteries. Later studies by Gosling and King (1974) showed that this pulsatility index could be represented by a simple formula of peak-to-peak velocity divided by mean velocity:

$$PI = \frac{Q_{max} - Q_{min}}{Q_{avg}} \tag{4.1}$$

Arterial obstructions damp the velocity waveform and reduce the pulsatility of blood flow along the artery, thus reducing the the peak-to-peak value and the PI. Also high mean flow rates decrease the PI.

The *inverse damping factor*, IDF, was introduced by Johnston et al. (1978) and is defined as the the ratio of the distal measured PI to proximal measured PI. The results showed that IDF increases toward the periphery and decreases with the severity of disease. This was in agreement with other methods' assessments of relating pressure drop to flow such as arm/calf pressure difference and strain gauge plethysmography. Also plotting the IDF with a fixed proximal PI and a varying distal PI against the

arterial segment length demonstrates the behavior of the normalized pulsatility index in proportionate detail making the plot easy to interpret.

Other flow related indices that can be applied to all arteries are the *Fourier pulsatility index*, PI_f, the *systolic-to-diastolic index*, PI_s, the *acceleration index*, ACI, which is a measure of the flow acceleration during systole, *half-width index*, HWI, and the *segmental systolic flow index*, ARI, which is the ratio of systolic flow in an artery containing a stenosis to a reference systolic flow not effected by the stenosis. For convenience in this study, the reference systolic flow will be taken from the proximal end of the brachial artery where the effect of a femoral stenosis is considered at the ankle. Typically the ARI is of use only in cases of varying stenoses rather than heart disease. The mathematical definition of these indices are:

$$PI_f = \sum_{i=1}^{n} \frac{Q_i^2}{Q_a^2} \tag{4.2}$$

$$PI_s = \frac{Q_p}{Q_d} \tag{4.3}$$

$$ACI = \frac{Q_p - Q_d}{\delta t_p} \frac{\tau}{Q_a} \tag{4.4}$$

$$HWI = \frac{\delta t_w}{\tau} \tag{4.5}$$

$$ARI = \frac{Q_p}{Q_{p(arm)}} \tag{4.6}$$

where Q_i is the amplitude of the i^{th} harmonic of the waveform, Q_a is the average flow, Q_p is the peak flow, Q_d is the diastolic flow value just before systole, τ is the period, δt_w is the width of the waveform halfway between Q_p and Q_d, δt_p is the width of the waveform between Q_p and Q_d, and $Q_{p(arm)}$ is the peak flow in the brachial artery. Clinical results have also revealed that these are useful sensitive indices (Fronek et al., 1973; Johnston and Taraschuk, 1976) in the case of severe stenosis. To determine

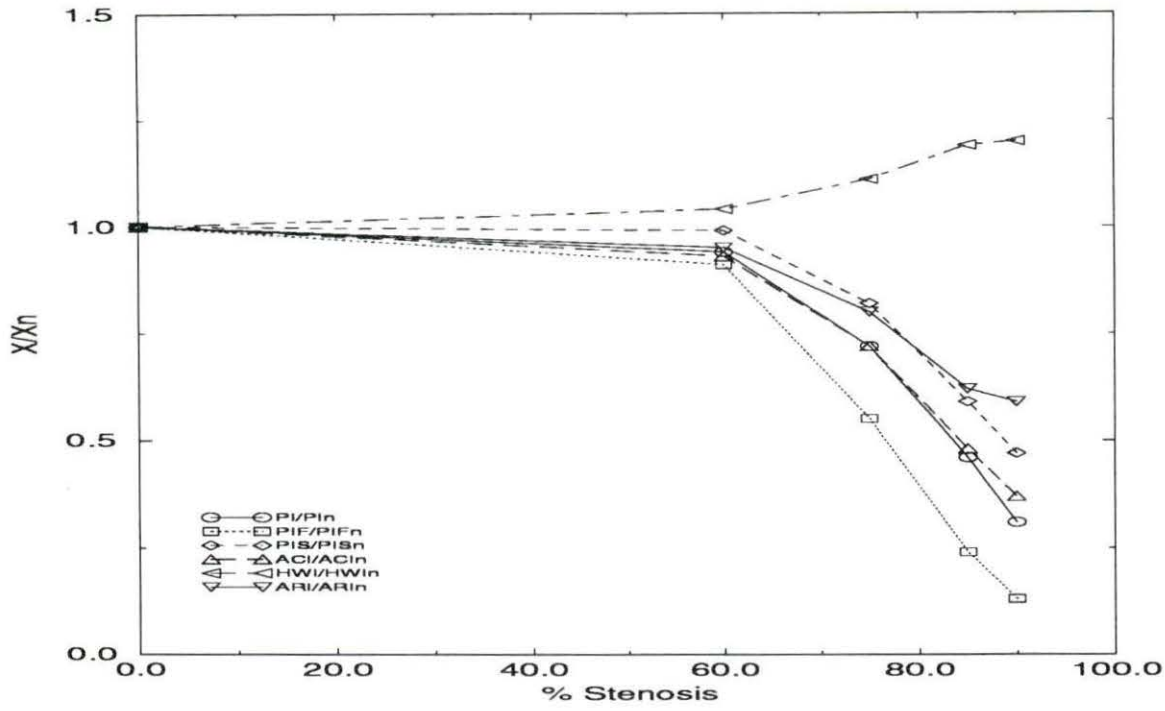

Figure 4.1: The effect of increasing stenosis severity in the L. femoral artery on various normalized flow indices measured in the L. posterior tibial artery (Stergiopulos et al., 1993)

each index's sensitivity to a particular stenosis or disease, the values are normalized to the control case to increase diagnosis objectivity for any individual person. In the graphs that follow the y-axis is denoted as X/Xn, where Xn is the value of a particular index under normal flow conditions, and X is the value of a particular index for any case. Stergiopulos et al. (1993) found that Eq. 4.5 is the least sensitive flow index to stenoses and that Eq. 4.1 and Eq. 4.2 are the most sensitive based on stenoses alone (Figure 4.1). One should note that the PI_s index would be ineffective for zero-flow cases.

Flow indices that are more sensitive to specific arterial regions, such as the carotid arteries, have also been developed. The carotid arteries have gotten the most

attention since these are the arteries that supply the brain. Pourcelot's (1974) pulsatility index is used for the the common and internal carotid arteries as a resistance index. Since the vessels of the brain normally have a very low resistance to blood flow, this index can detect a thrombosis if the value increases with increasing distal resistance. Archie's index (1981) involves a comparison between the two common carotid arteries and is very specific in predicting carotid disease, and Roederer et al. (1982) developed an index to predict disease in the carotid bifurcation. In this research, only the indices that may be used generally throughout the body will be more closely examined.

Since flow tracings are much easier to obtain non-invasively than pressure tracings, flow indices alone were investigated in this research. Indices can be very helpful in detecting the presence of arterial disease, but they must be applied judiciously. In determining indices from a flow waveform it is essential that no artifacts are present in the waveform so that index calculations are not inaccurate. For instance a false maximum or minimum flow velocity due to instability in the flow may be taken as the actual maximum or minimum value, which could severely alter the index calculations. Index values should be compared to established confidence values based on the equipment and techniques used in each investigator's research, as well as to the pressure and flow waveforms. When more than one index is used for the same diagnosis, it is important to keep in mind what each index measures because each is sensitive to different flow values.

CHAPTER 5. METHODS AND RESULTS OF STENOSIS AND HEART DISEASE CASES ON WAVEFORMS AND INDICES

Methods

Using the arterial model of Stergiopulos et al. (1992) modified by incorporating the new compliance-pressure relationship and the inclusion of the appropriate flow indices discussed below, the following will be studied:

1. A comparison of flow and pressure waveforms using a pressure proximal boundary condition (Balar et al., 1989) versus a flow proximal boundary condition used by Stergiopulos et al. (1992).

2. A comparison of waveform solutions using different wall shear coefficients.

3. A comparison of flow indices using different proximal boundary conditions and different wall shear coefficients with a stenosis in the femoral artery.

4. A comparison of flow index values of different heart pulses for various diseased conditions.

(Note: The model parameters were not changed for the hypertensive case where compliance and terminal impedance would normally be affected. Instead, a hypertensive pressure waveform was used for the proximal boundary condition and the state of the

remaining arterial system was maintained at normal conditions, which would affect the accuracy of this model for hypertension.)

Several clinically significant cases were run to show the effectiveness of various indices detecting cardiovascular diseases or disorders at various points in the body. These cases included stenoses of 60%, 75%, 85%, and 90%, hypertension (HYP), valvular aortic stenosis (AS), pure aortic regurgitation (AI), and a combination of aortic regurgitation and valvular aortic stenosis (AS/AI). The indices selected to observe their sensitivities to the various flow abnormalities are the pulsatility index (PI), the Fourier pulsatility index (PI_f), the systolic-to-diastolic index (PI_s), the acceleration index (ACI), and the segmental systolic flow index (ARI) for stenosis only. These indices were normalized to the control case at its respective node to show the sensitivity of each index to a change in the initial flow waveform.

To validate the sensitivity of the indices, the pressure and flow pulses are taken at the distal left posterior tibial artery for a stenosis in the left femoral artery . Measurements are taken at a variety of locations for the other disease cases. The points that were arbitrarily chosen to represent the extremities include the right external carotid artery (neck), the distal right radial artery (wrist), and the distal left posterior tibial artery (ankle). All of these points represent locations where flow can easily be measured by ultrasonic flow meter devices. Although Stergiopulos et al. (1992) used the same general concepts as Porenta et al. (1986), Balar et al. (1989), and Weerappuli (1987) on which to base his blood flow model, these other authors placed the proximal boundary condition at the beginning of the arterial segments they were investigating. Thus their data may look somewhat different from that of this research since they did not take into the account effects of the pulse waveform

emanating through the body before reaching a particular segment of interest. Also, the new compliance relationship used in this study will change some of the data when comparing Stergiopulos' original work to that in this paper. Hence, an index baseline (see Figure 4.1) will be established using his original data where the proximal boundary condition was a flow input and wall shear stress coefficients equal to 1.0. All variations between their normalized indices and those calculated by this program under the same conditions may then be attributed to the new compliance relationship.

Control Case

Flow and pressure waveforms for the left and right external carotid artery (nodes 74 and 56), the left and right distal node of the radial artery (nodes 101 and 35), and the left and right distal node of the posterior tibial artery (nodes 195 and 231) are shown in Figures 5.1, 5.2, 5.3, 5.4, 5.5, and 5.6, respectively. These are shown over three cycles using a pressure input at the ascending aorta for the proximal boundary condition, a time step of $\Delta t = 0.0001$, and varying the wall shear coefficients c_u and c_v along each segment under normal flow conditions. Stergiopulos et al. (1992, 1994) have validated the accuracy of this program using a flow input, wall shear coefficients of 1.0, and a non-linear compliance-pressure relationship. Initial comparisons in the waveforms seem to be similar in general trend (also see section on pressure vs. flow input later in this chapter).

Since flow indices are the primary emphasis of this research, flow waveforms will be of more importance for discussion. General characteristics that are commonly found in the systemic circulation are exhibited in the computed waveforms. Wave reflection is evident during diastole in the peripheral pressure pulses, back flow is ex-

hibited for a small fraction of the cycle, there is a definite time delay as the pressure and flow pulses emanate to the periphery, flow pulse is damped as the pulse propagates along the vascular tree and mean flow is reduced as a direct effect of branching, and there is significant amplification of the pressure pulse (although mean pressure drops) as the pulse propagates to the periphery. Since there is no smooth transition from one segment to another at branches in this model, over-amplification of the wave is evident. Again, some variations in the data throughout the body may occur when comparing these simulations to other authors' values as a result of the proximal boundary condition emanating from the heart rather than beginning at a particular limb, as well as artery geometries being slightly different. Other deviations between experimental in vivo waveforms and simulated waveforms are mainly attributed to the incomplete description of the full arterial tree (where only major arteries are included in this model), errors in assumptions of branch conditions, boundary conditions, and model parameter estimations.

Results

Sensitivity Comparisons

Flow Input vs. Pressure Input Comparisons of trends of a normal pressure input to a normal flow input at the root of the ascending aorta are shown in Figures 5.7 and 5.8 for a prescribed or calculated pressure and flow waveform, depending on the proximal boundary condition. The Fourier coefficients for the normal proximal flow waveform were taken from a waveform from Nichols et al. (1977) while the Fourier coefficients for the normal proximal pressure waveform were taken from a waveform from Mason et al. (1964). In both cases the wall shear coefficients are

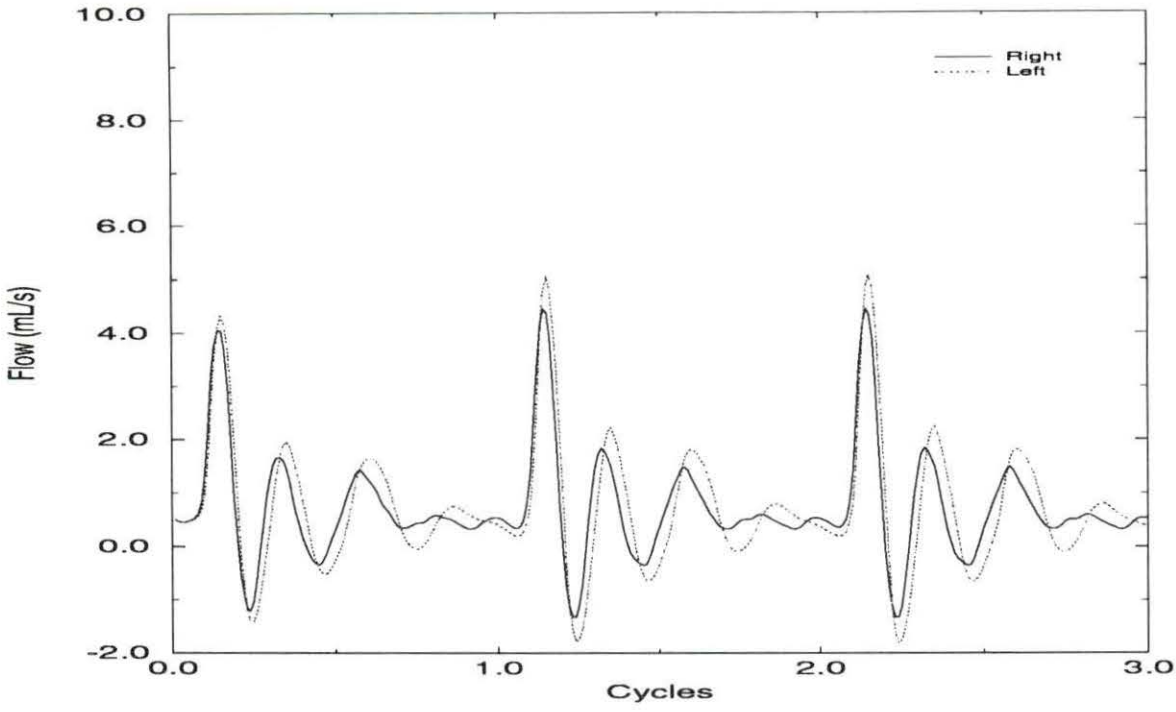

Figure 5.1: Flow pulses in R. and L. external carotid using pressure input

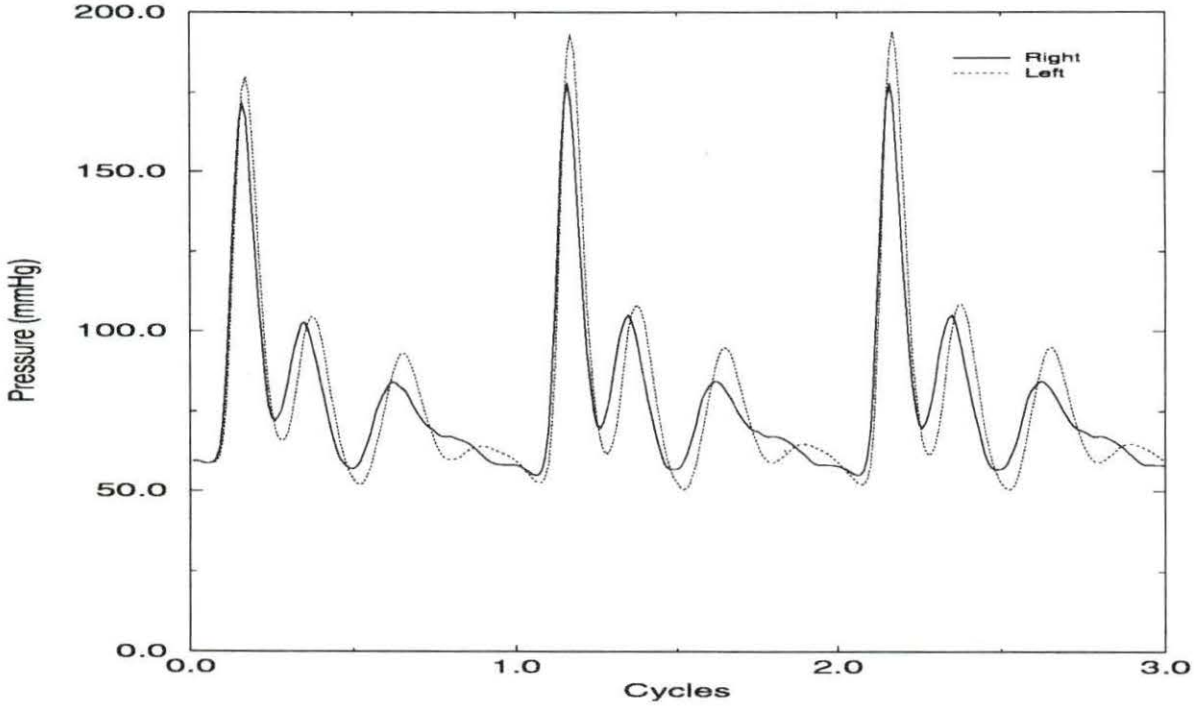

Figure 5.2: Pressure pulses in R. and L. external carotid artery using pressure input

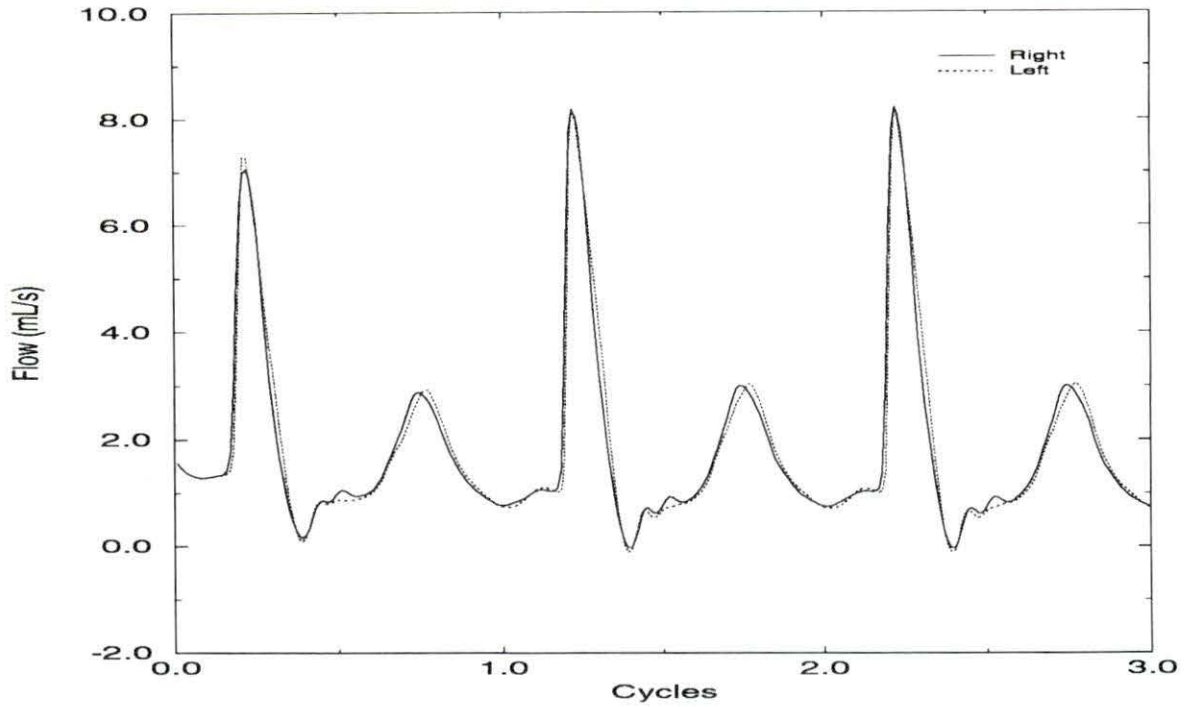

Figure 5.3: Flow pulses in R. and L. radial artery

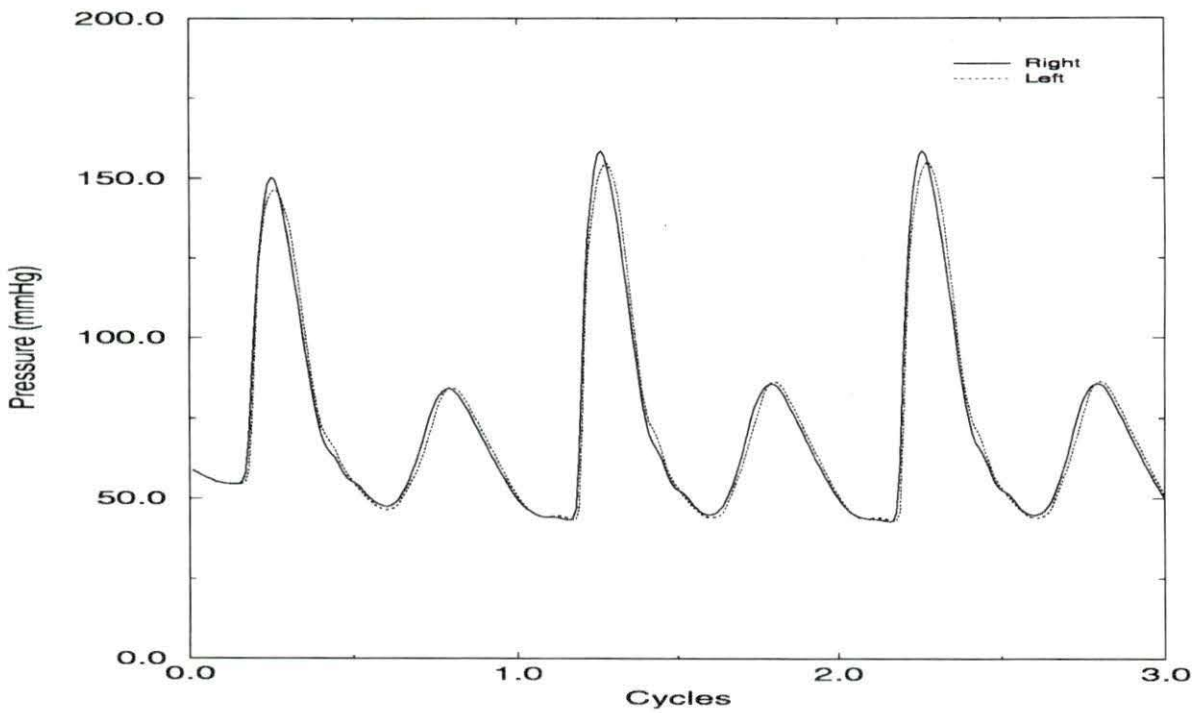

Figure 5.4: Pressure pulses in R. and L. radial artery

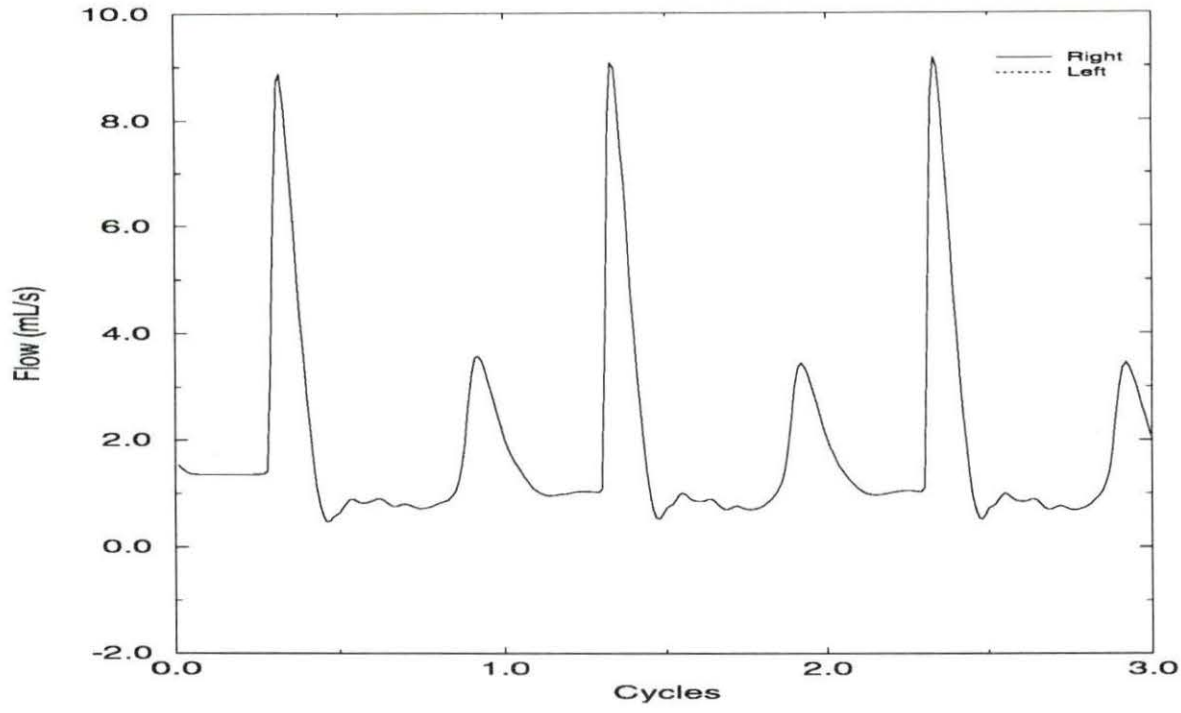

Figure 5.5: Flow pulses in R. and L. posterior tibial artery

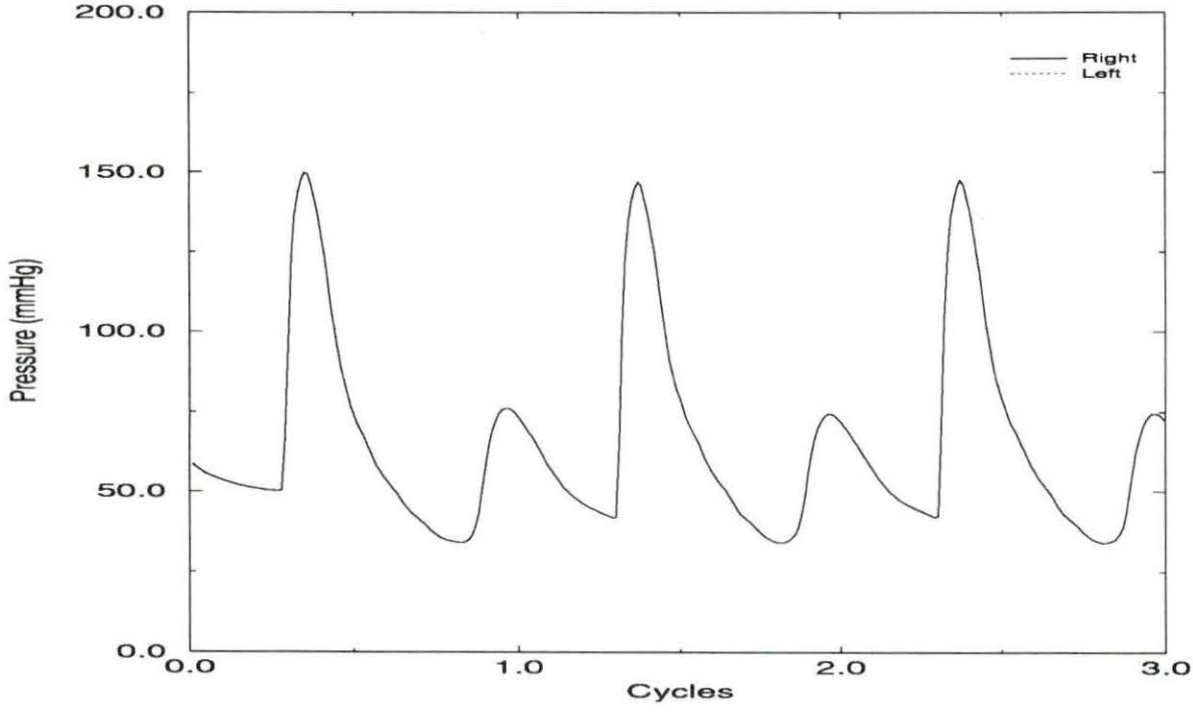

Figure 5.6: Pressure pulses in R. and L. posterior tibial artery

taken to be $c_u = 1.0$, $c_v = 1.0$ and the waveform is taken from the the third cycle, where the effects of the erroneous initial conditions are completely damped out and the solution is assumed to converge. As can be seen, the trends in all waveforms are similar although the flow input exhibits a more stable flow waveform. The zero-flow portion of the ascending aortic flow that normally takes place during diastole was not accurately resolved using pressure as the proximal boundary condition, and amplitude of the flow tends to be amplified. Nevertheless, pressure will be used as the proximal boundary condition since aortic pressure inputs for various cases of heart disease were readily available from the literature (Mason et al., 1964). Stergiopulos et al. (1992) do verify that their program is qualitatively accurate in replicating actual arterial pulse shapes using a pressure input.

Constant Wall Shear Coefficients vs. Variable Wall Shear Coefficients

The wall shear coefficients are never constant values in the arterial systems, hence, the effect these coefficients have on the waveforms, especially the flow, is an important consideration. Figures 5.9 and 5.10 show the effect that calculating c_u and c_v for each node has on the waveforms for a pressure input as opposed to keeping these coefficients constant at 1.0 throughout the entire arterial tree. Stergiopulos et al. (1992) already determined that increasing the c_u will cause a phase shift of the waveform, whereas an increase in c_v will dampen the flow magnitude. The ascending aorta, the calculated wall shear coefficients of which are $c_u = 1.1$ and $c_v = 3.5$, has the largest α parameter and thus is where the c_v would be the largest. As a result, one would expect more damping in the aorta flow waveform if the α parameter is allowed to change rather than setting it at a constant value of 1.0. Figure 5.9 shows

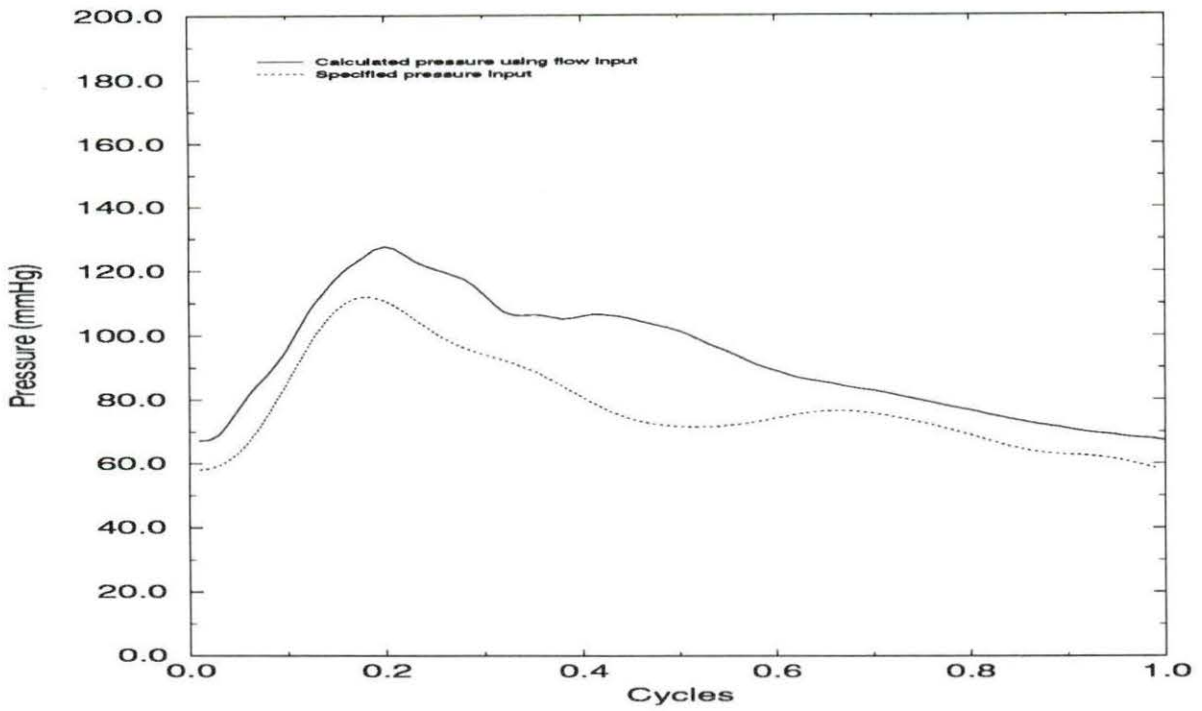

Figure 5.7: Comparative normal pressure pulses at the root of the ascending aorta

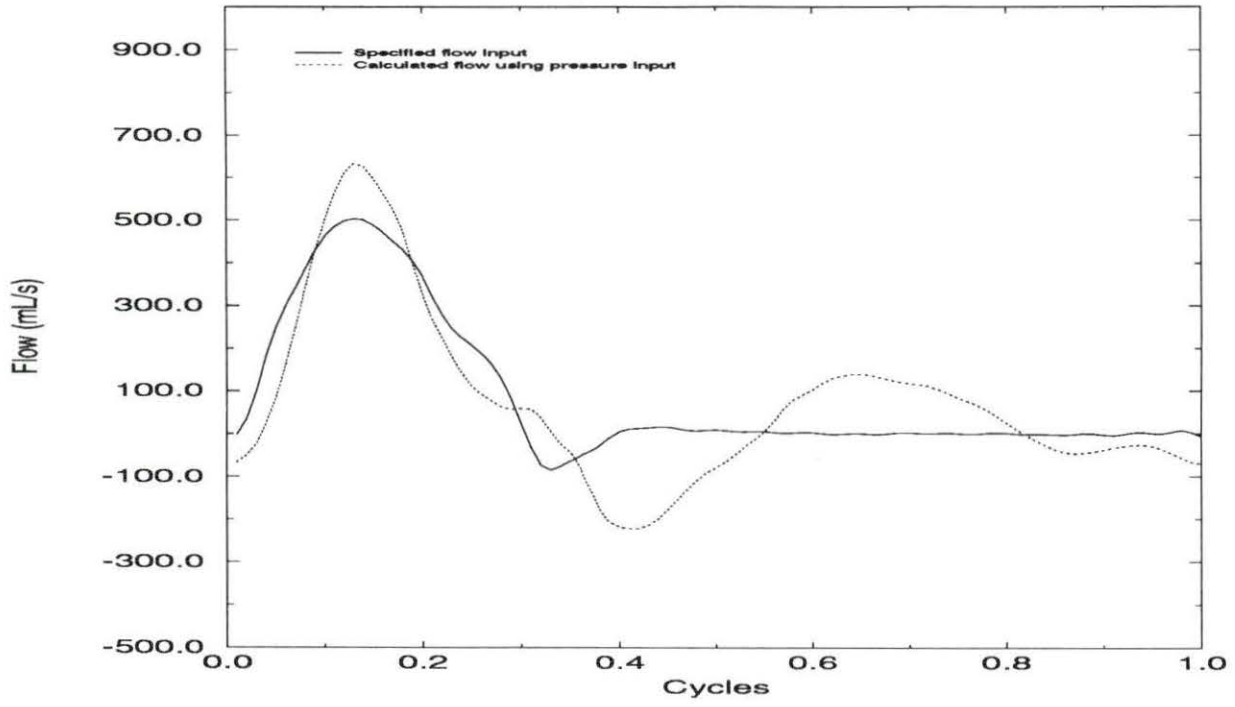

Figure 5.8: Comparative normal flow pulses at the root of the ascending aorta

that the peak flow is damped by approximately 30 mL/s. Damping is not very noticeable since the area is so large, which disperses the shear stress. In the tibial arteries, the α parameter is very small (c_u and c_v are calculated to be 1.3 and 1.0, respectively), thus c_u is larger than 1.0, which acts to shift the waveform. It is interesting to note that there is some residual damping of the posterior tibial artery waveform by 1 mL/s. This may be due to the fact that the unsteady and viscous wall shear coefficients are allowed to change as the pulse propagates through the systemic circulation and affects the peripheral waveforms. As stated in Stergiopulos et al. (1992), the effects of recalculating the wall shear coefficients at each node as opposed to keeping the values constant makes a negligible difference on the flow waveforms. The main benefit of varying the wall shear coefficients at this point in the study is a more realistic computer model. Its effect on the flow indices will be discussed in the section on stenoses.

Stenosis and Indices

A stenosis chosen to be 2 cm in length and varying in area occlusion percentage is placed 20 cm from the proximal end of the left femoral artery. The pressure and flow waveforms are simulated in the distal left posterior tibial artery for cases of 60%, 75%, 85%, and 90% occlusion as shown in Figures 5.11 and 5.12 for pressure input. Vasodilation comes into effect beginning at approximately 60% and is no longer effective in maintaining the mean flow after approximately 75% in the posterior tibial artery when terminal resistance has reached its maximum reduction of 20%. Otherwise, for 90% stenosis, the peripheral resistance would have to decrease by +60% to maintain constant mean flow (Fig. 5.13). The particular percentage of the

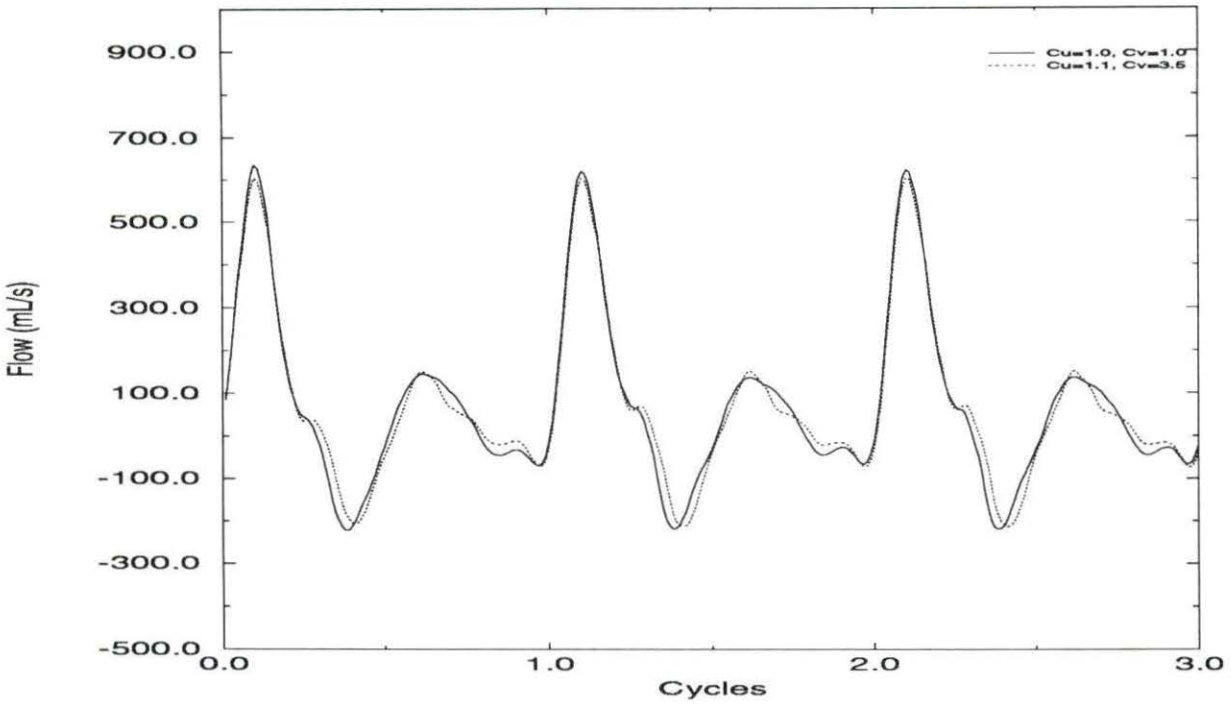

Figure 5.9: Flow sensitivity to a change in c_v in the ascending aortic arch

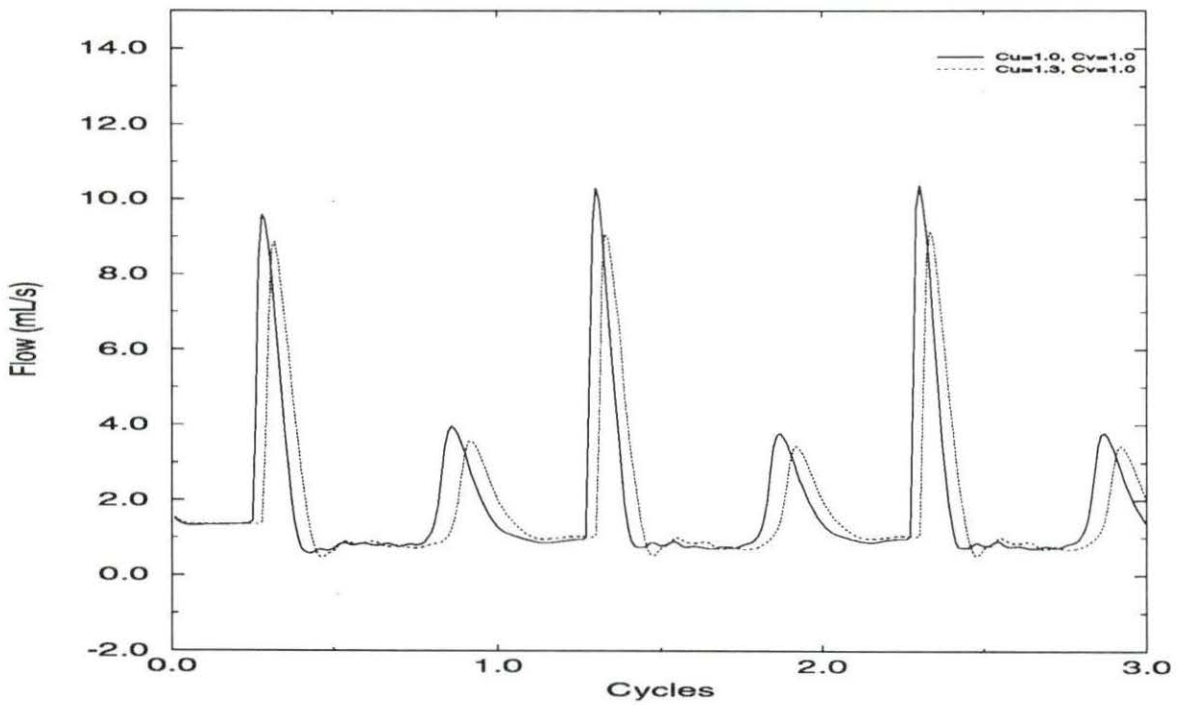

Figure 5.10: Flow sensitivity to a change in c_u in the L. posterior tibial artery

critical stenosis depends on the location of the stenosis. Thus it is important that vasodilation be accounted for in the model before taking the flow indices from the waveforms. An example of the effect of keeping the terminal peripheral resistances constant as opposed to incorporating autoregulation on the flow indices is shown in Fig. 5.14 for PI. The normalized indices are slightly larger in the case of constant terminal resistance as a result of the mean flows being allowed to decrease by keeping peripheral resistance constant.

Wall shear coefficients and using a flow input versus a pressure input for the proximal boundary condition affect the flow indices each in their own way. Since the validity of the original computer model was based on a quadratic pressure-area relation, and using a flow input case with all wall shear coefficients set to 1.0 (Stergiopulos et al., 1993), this will be used as a base line to measure the accuracy of indices taken from waveforms that use a pressure input with both wall shear coefficients set to 1.0, as well as varying wall shear coefficients for both flow and pressure inputs. Figures 5.15, 5.16, 5.17, 5.18, and 5.19 compare each case for the normalized indices, PI, PI_s, PI_f, ACI, and ARI, respectively. Vasodilation is accounted for in each case and a line is drawn between each point to emphasize sensitivity.

In all cases, the normalized indices reveal that with increasing stenosis severity, each index decreases in a nearly exponential fashion, and that the new compliance relationship does affect the indices since all are less than the baseline. The special exception was the acceleration index. ACI was the most difficult to calculate accurately because its sensitivity is dependent on a very precise reading of the time between peak systole and end diastole. An increase or decrease in time of 0.01 can dramatically increase or decrease the value of ACI. The Fourier pulsatility index stands out as

being the most sensitive to stenosis since it decreases the most. Varying wall shear coefficients tend to increase the values of the indices and decrease the overall sensitivity of each index. Thus it is important, when using the new compliance relationship (Eq. 2.22), to vary the nodal wall shear coefficients accordingly because it will affect the sensitivity and accuracy of the indices even though the waveform does not seem to change much. The effect of using a flow input as opposed to a pressure input for the proximal boundary condition is inconsequential on the index results, as expected, since both index values are nearly identical using similar wall shear coefficients.

Diseased Heart Conditions and Indices

Figures 5.20 displays the pressure waveforms for various types of heart disease, and 5.21 shows the resulting flow waveforms at the proximal root of the ascending aorta where the wall shear coefficients were varied according to the alpha parameter. These waveforms vary dramatically from the normal flow case in their shape and size. Tables 5.1, 5.2, 5.3 reflect the effect the various disease cases have on the flow indices PI, PI_f, PI_s, and ACI at the external carotid, radial, and posterior tibial artery (see Figures 5.22, 5.23, 5.24, 5.25, and 5.26 for flow pulses of diseased heart conditions). In the following sections, each disease case will be discussed for the selected indices and extremity locations to validate their predicting ability, as well as to see if any particular index is more sensitive to a disease case than another. The normalized diseased case index value is subtracted from the normalized control value (equal to one) when discussing a percent change:

$$\frac{Control - Diseased}{Control} \times 100.$$

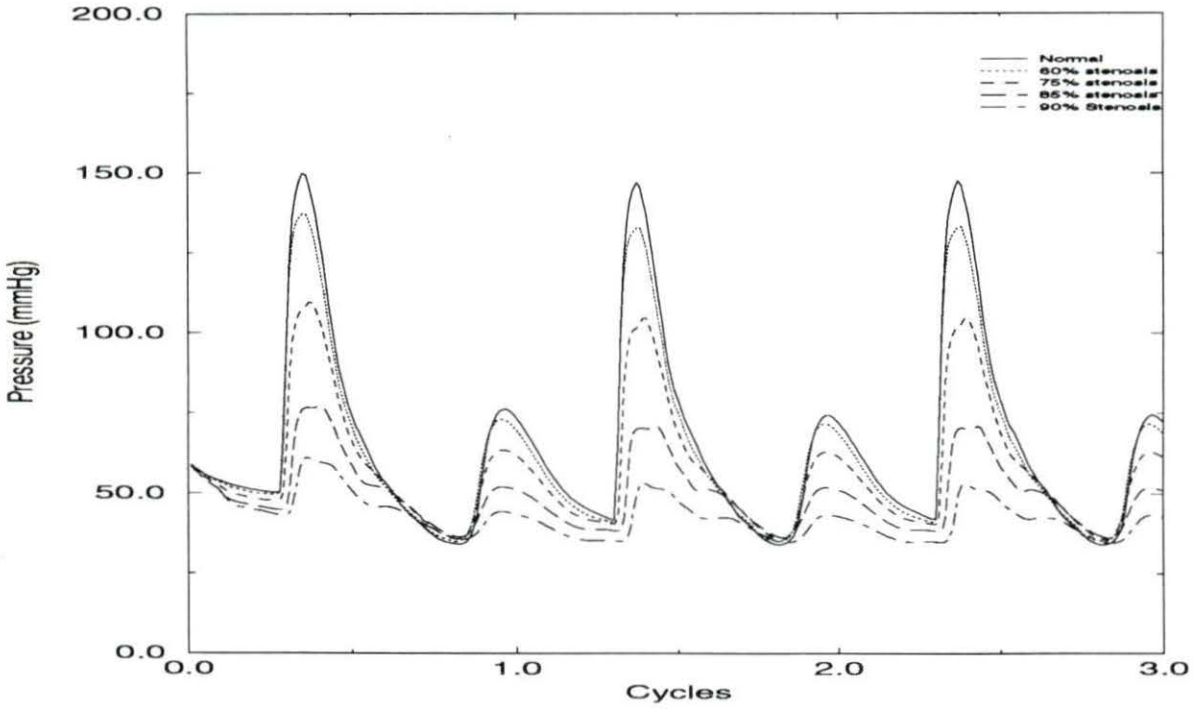

Figure 5.11: Effect of severity of L. femoral stenosis on L. posterior tibial pressure

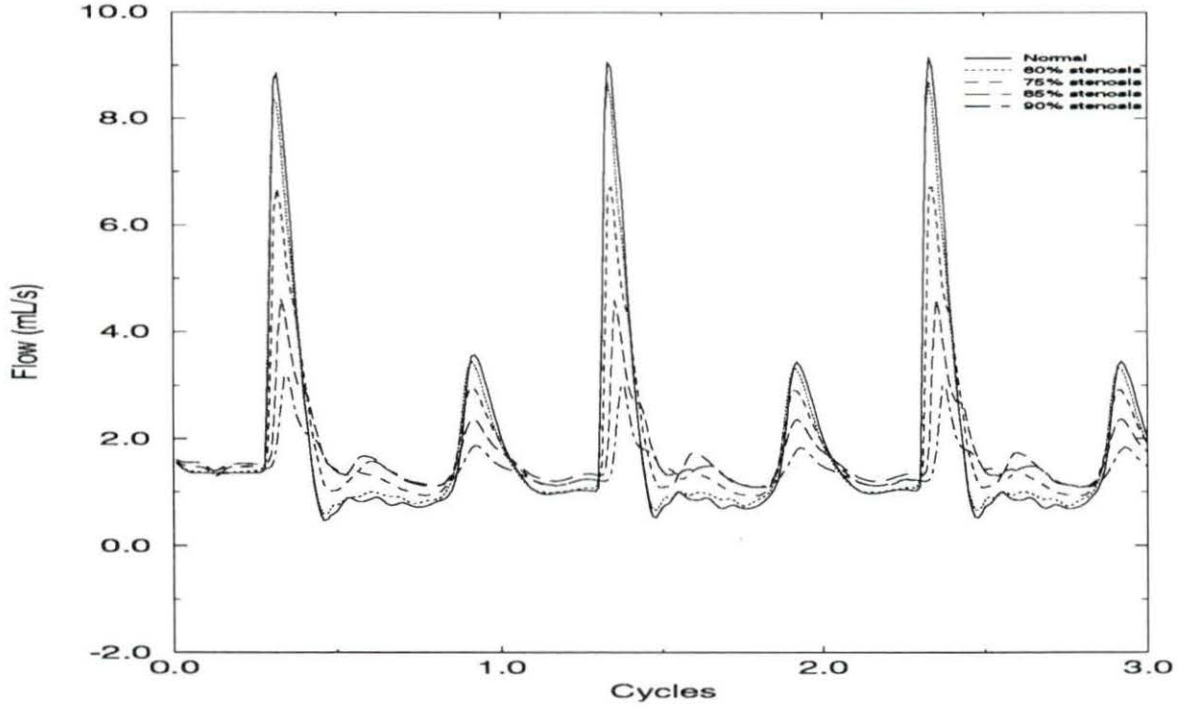

Figure 5.12: Effect of severity of L. femoral stenosis on L. posterior tibial flow

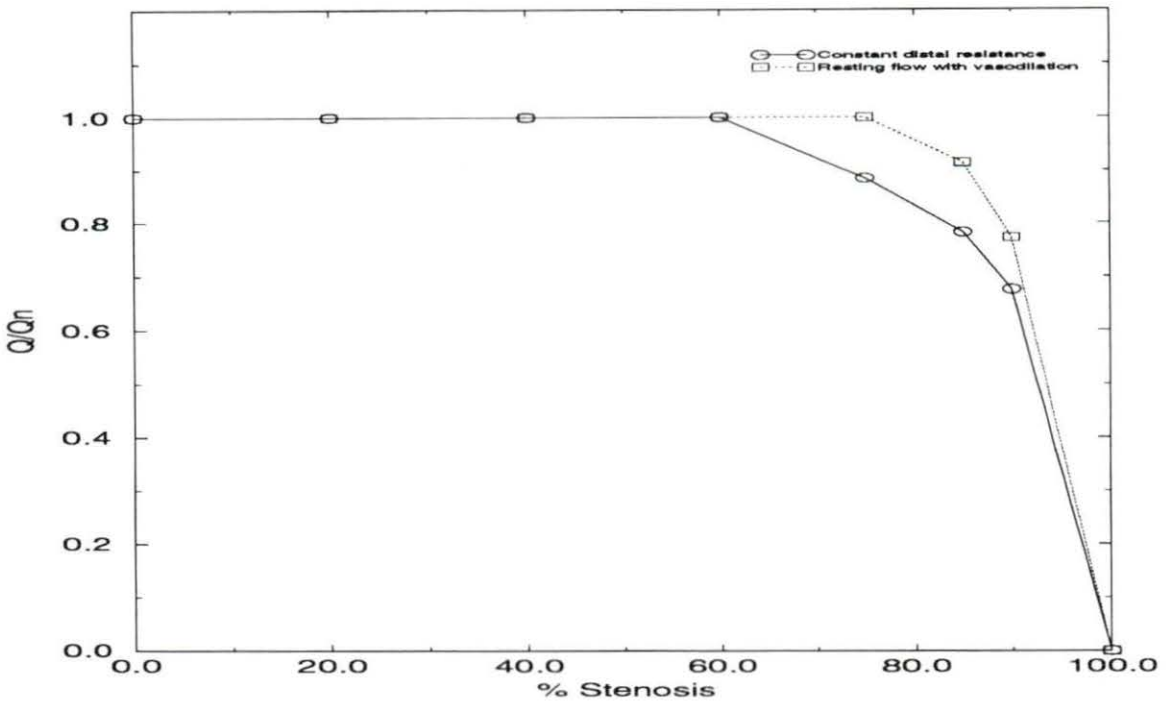

Figure 5.13: Effect of femoral stenosis and vasodilation on regional mean blood flow. Q_n denotes normal flow.

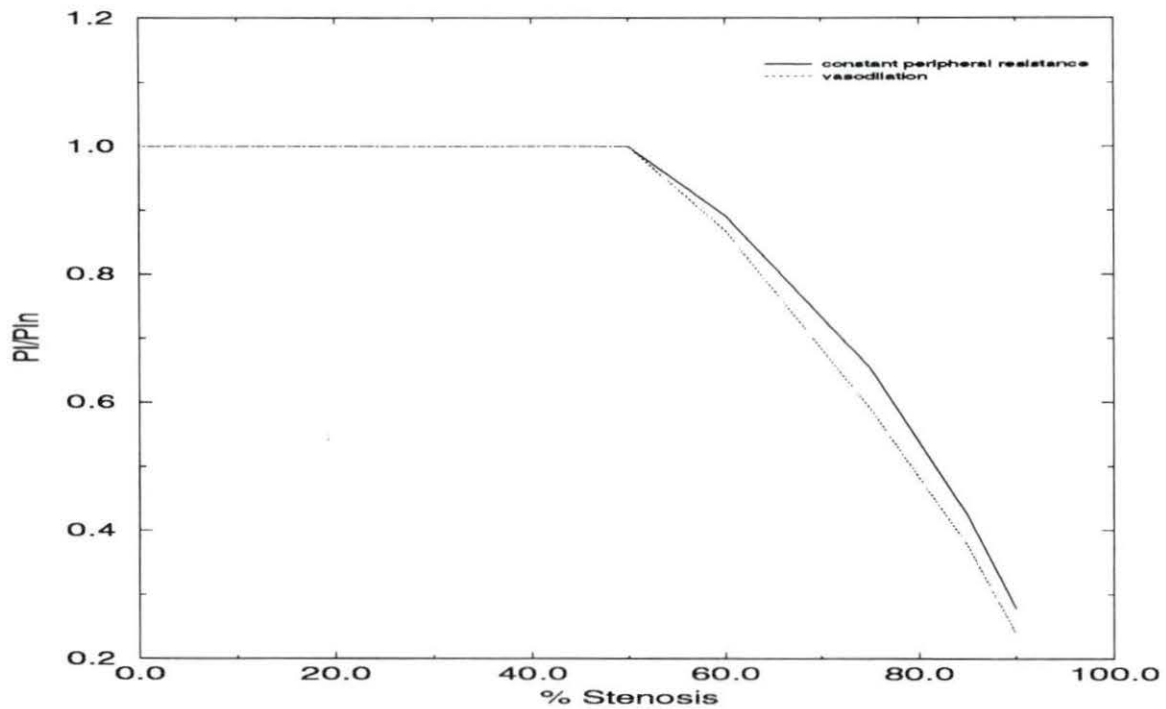

Figure 5.14: Index sensitivity to vasodilation in the L. posterior tibial artery. PI_n denotes the PI under normal flow conditions.

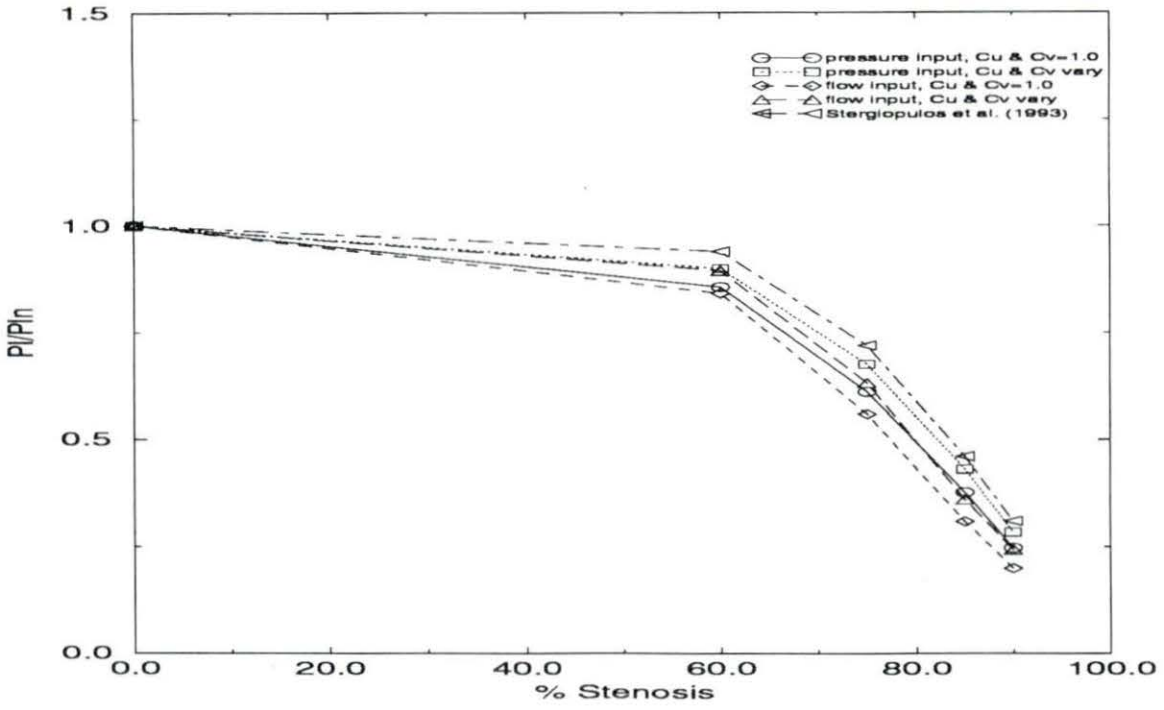

Figure 5.15: Effect of severity of L. femoral stenosis on L. posterior tibial pulsatility index, PI.

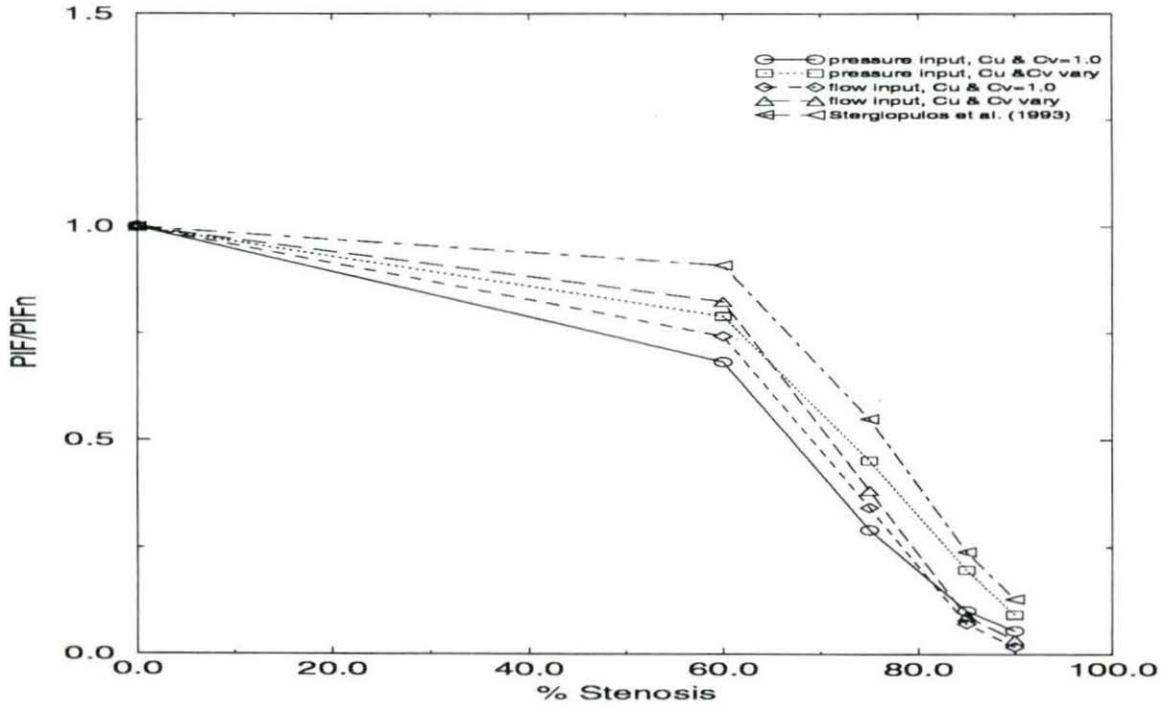

Figure 5.16: Effect of severity of L. femoral stenosis on L. posterior tibial Fourier pulsatility index, PI_f.

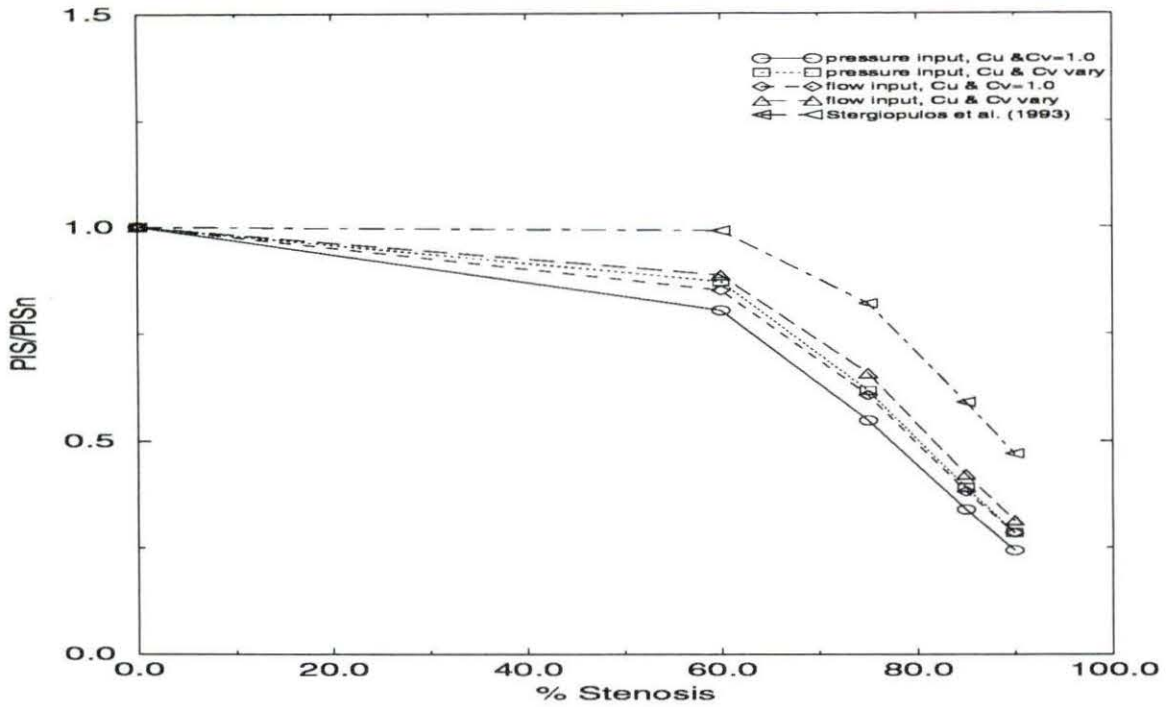

Figure 5.17: Effect of severity of L. femoral stenosis on L. posterior tibial systolic-to-diastolic index, PI_s.

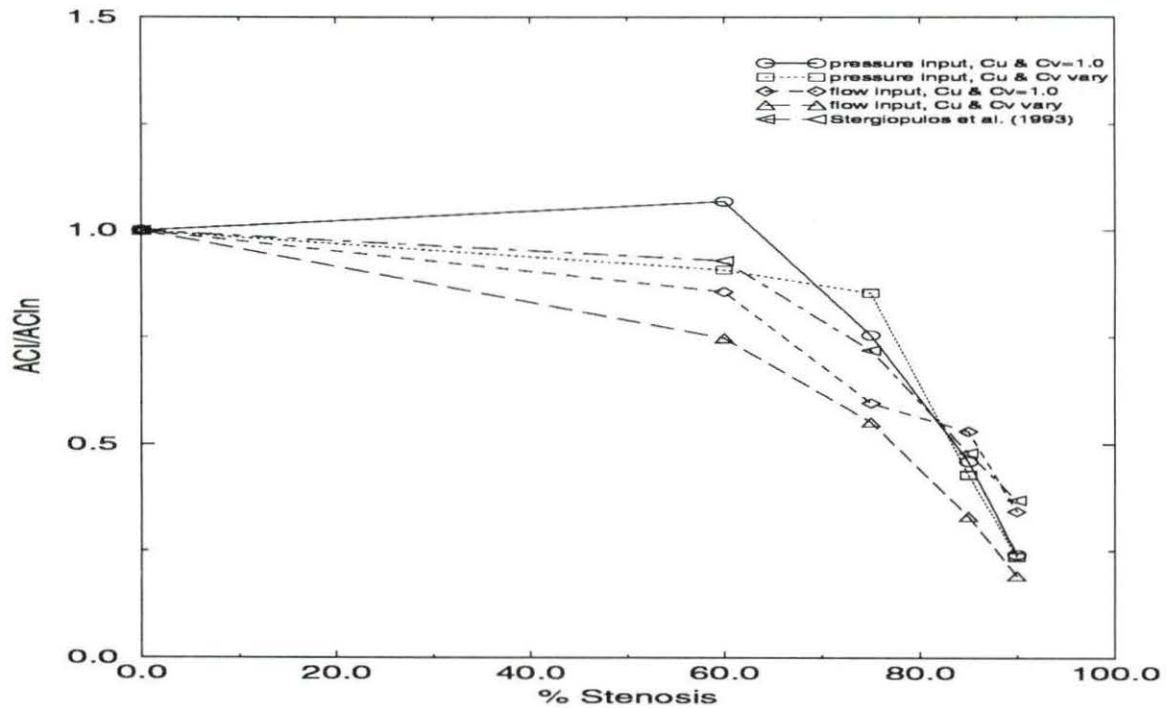

Figure 5.18: Effect of severity of L. femoral stenosis on L. posterior tibial acceleration index, ACI.

Table 5.1: Normalized flow indices for various cases of heart disease calculated at the R. external carotid artery

Case	$\frac{PI}{PI_n}$	$\frac{PI_f}{PI_{fn}}$	$\frac{PI_s}{PI_{sn}}$	$\frac{ACI}{ACI_n}$
Control	1.0000	1.0000	1.0000	1.0000
HYP	0.1965	0.0685	0.3154	0.1789
AS	0.4471	0.3467	0.5340	0.3908
AI	1.3299	1.6702	15.7004	1.8357
AS/AI	0.9890	1.5006	1.0076	1.5037

Table 5.2: Normalized flow indices for various cases of heart disease calculated at the R. radial artery

Case	$\frac{PI}{PI_n}$	$\frac{PI_f}{PI_{fn}}$	$\frac{PI_s}{PI_{sn}}$	$\frac{ACI}{ACI_n}$
Control	1.0000	1.0000	1.0000	1.0000
HYP	0.4070	0.1870	0.4647	0.1952
AS	0.5356	0.4532	0.6574	0.2486
AI	0.9771	0.6690	1.8293	1.2543
AS/AI	0.5763	0.2905	0.9755	0.9280

Table 5.3: Normalized flow indices for various cases of heart disease calculated at the L. posterior tibial artery

Case	$\frac{PI}{PI_n}$	$\frac{PI_f}{PI_{fn}}$	$\frac{PI_s}{PI_{sn}}$	$\frac{ACI}{ACI_n}$
Control	1.0000	1.0000	1.0000	1.0000
HYP	0.5460	0.2258	0.5691	0.2250
AS	0.7602	0.7100	0.6808	0.4718
AI	1.0514	1.2175	1.3758	1.3823
AS/AI	0.6460	1.9192	1.0192	0.8099

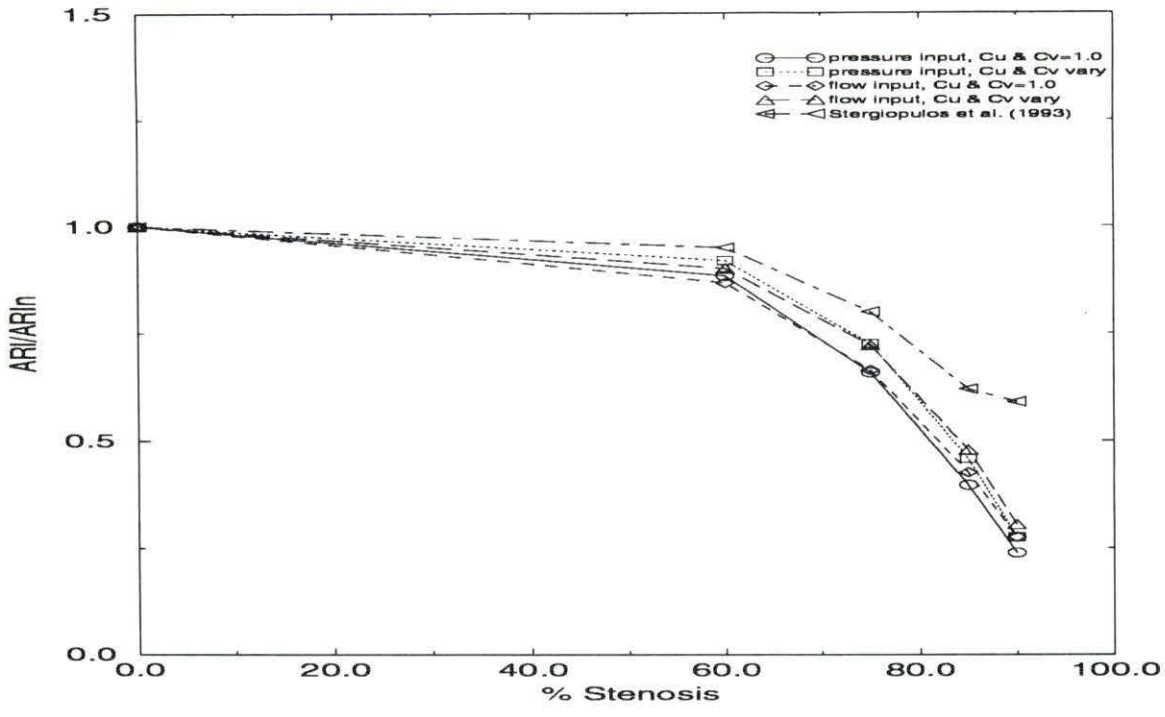

Figure 5.19: Effect of severity of L. femoral stenosis on L. posterior tibial ankle/arm flow index, ARI.

Hypertension During hypertension, heart rate is decreased to approximately 71 beats/min from control. Hypertension creates an aortic flow pulse that is characterized by a reduced maximum and minimum flow (back flow) amplitude, an increased mean flow, a reduced end diastolic flow magnitude, a slower rise in systolic flow (slope), and a prolonged systolic phase, although the systolic and diastolic pressure are greatly elevated from the control case. As the pulse travels further from the heart, mean flow continues to increase because peak flow amplitude approaches that of the control case. It should be noted that in this model no parameter values such as compliance or terminal impedance data were changed, but probably should change for hypertension. The systolic duration also approaches that of the control case as the pulse travels further from the heart. From the index tables for the case of

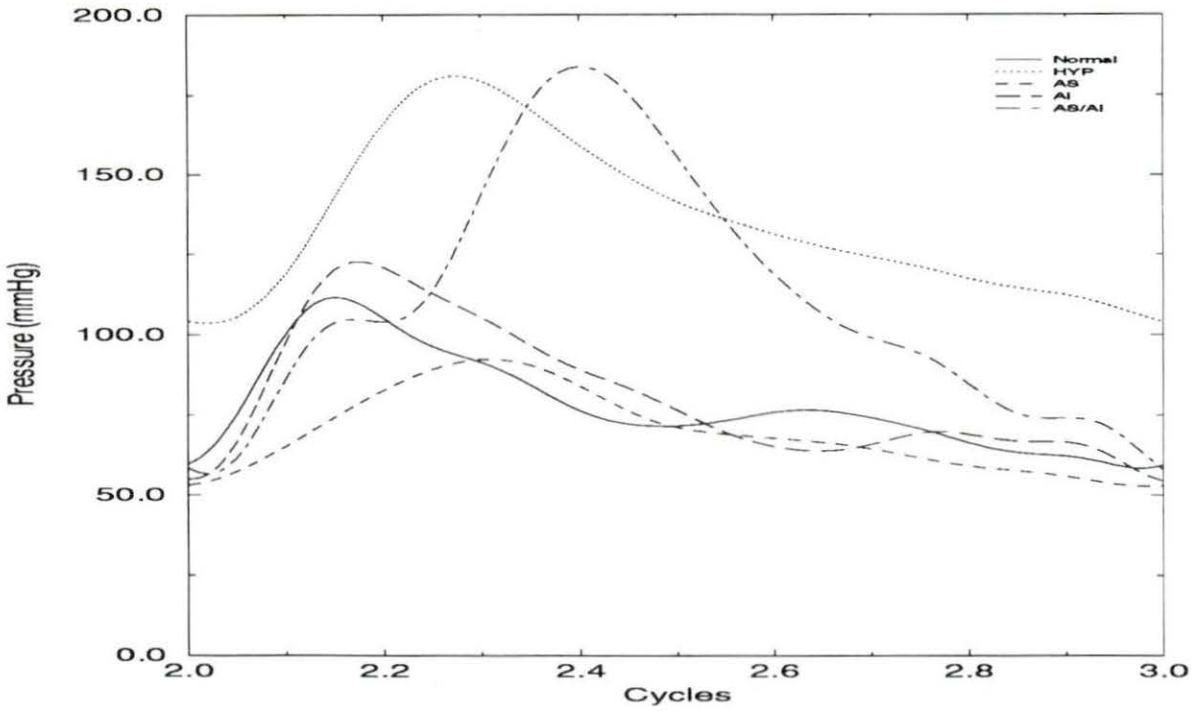

Figure 5.20: Prescribed pressure pulse at proximal root of ascending aorta for various heart diseases

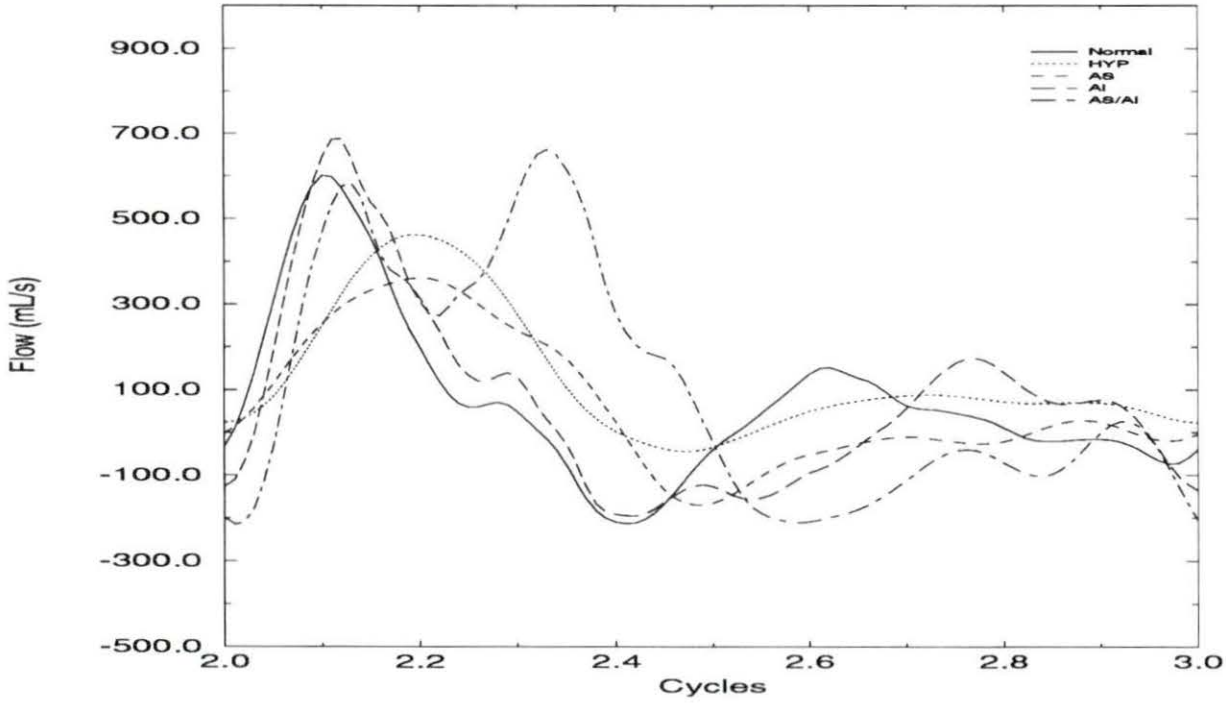

Figure 5.21: Calculated flow pulse at proximal root of ascending aorta for various heart diseases

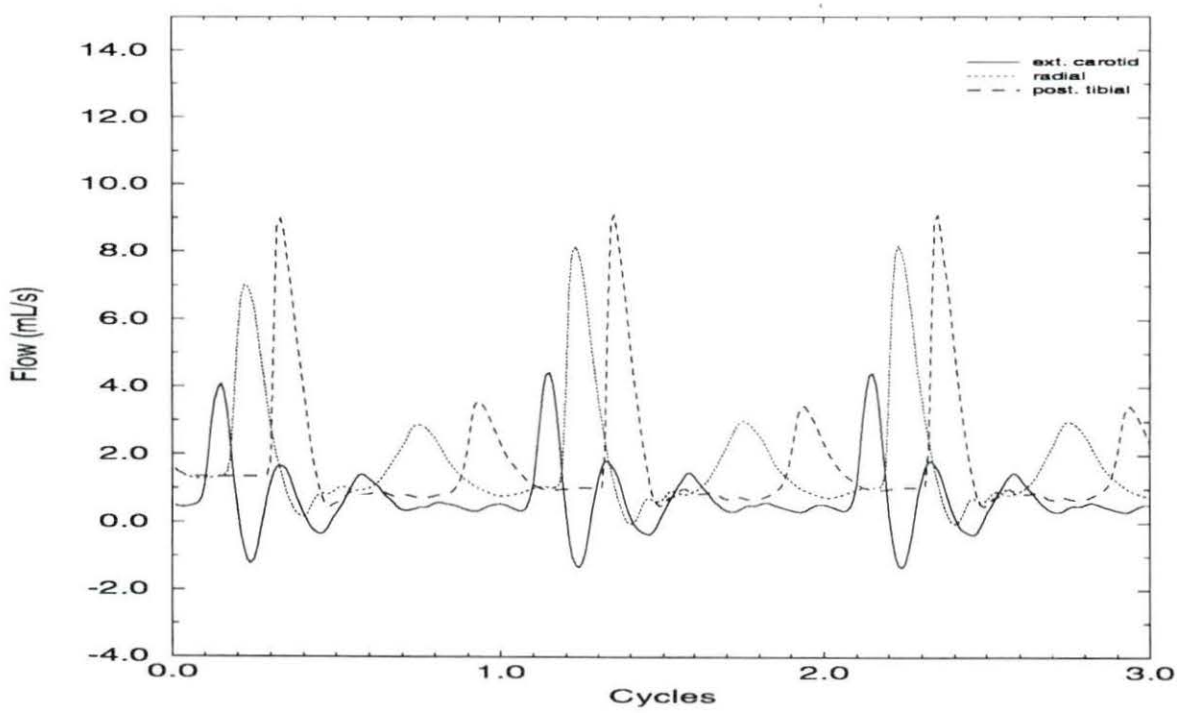

Figure 5.22: Flow pulses measured at various locations for the control case

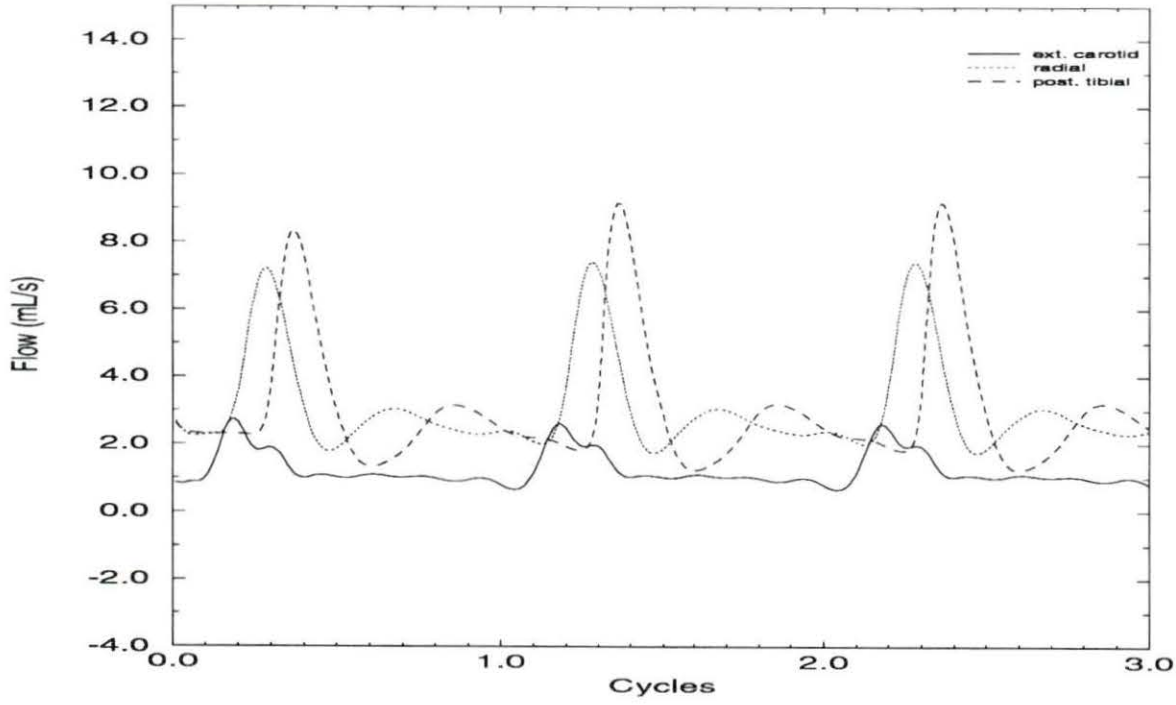

Figure 5.23: Flow pulses measured at various locations for hypertension (HYP).

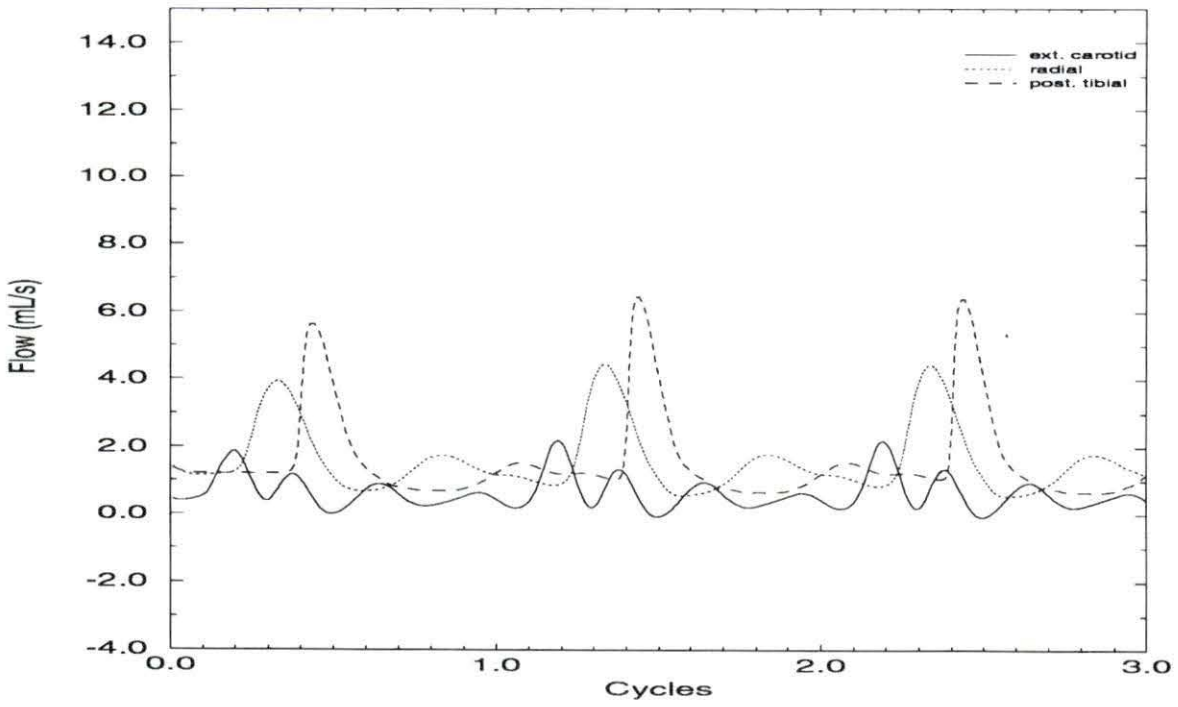

Figure 5.24: Flow pulses measured at various locations for valvular aortic stenosis (AS).

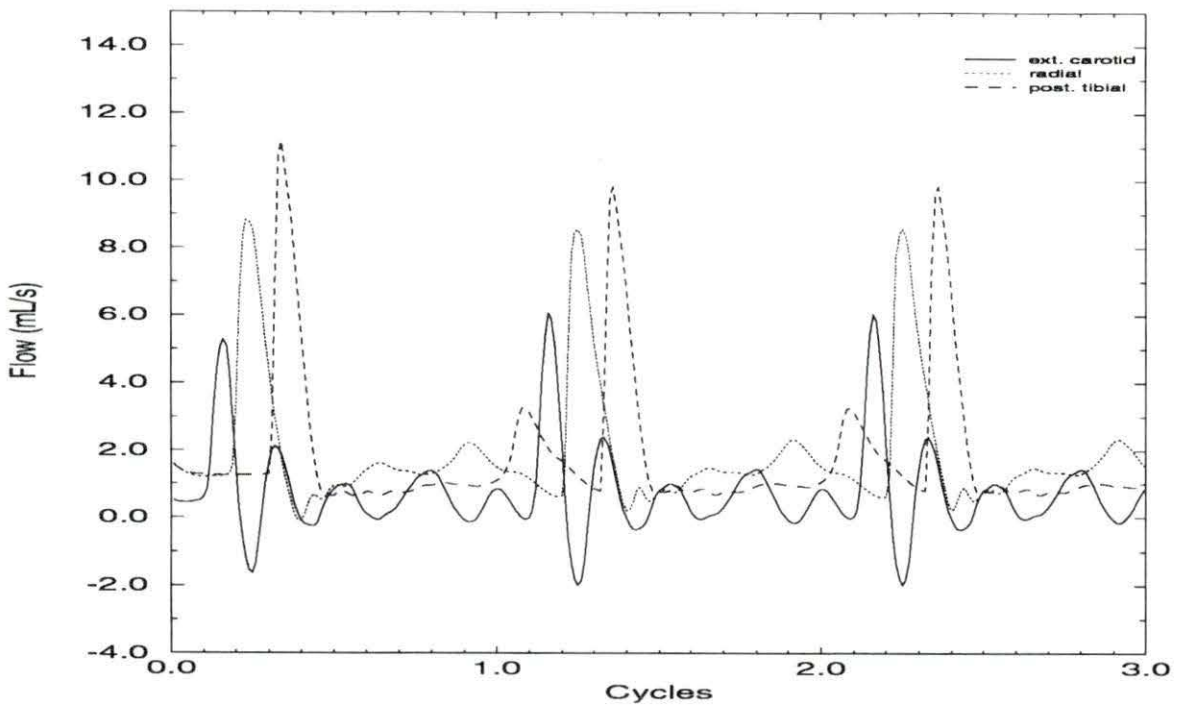

Figure 5.25: Flow pulses measured at various locations for aortic regurgitation (AI).

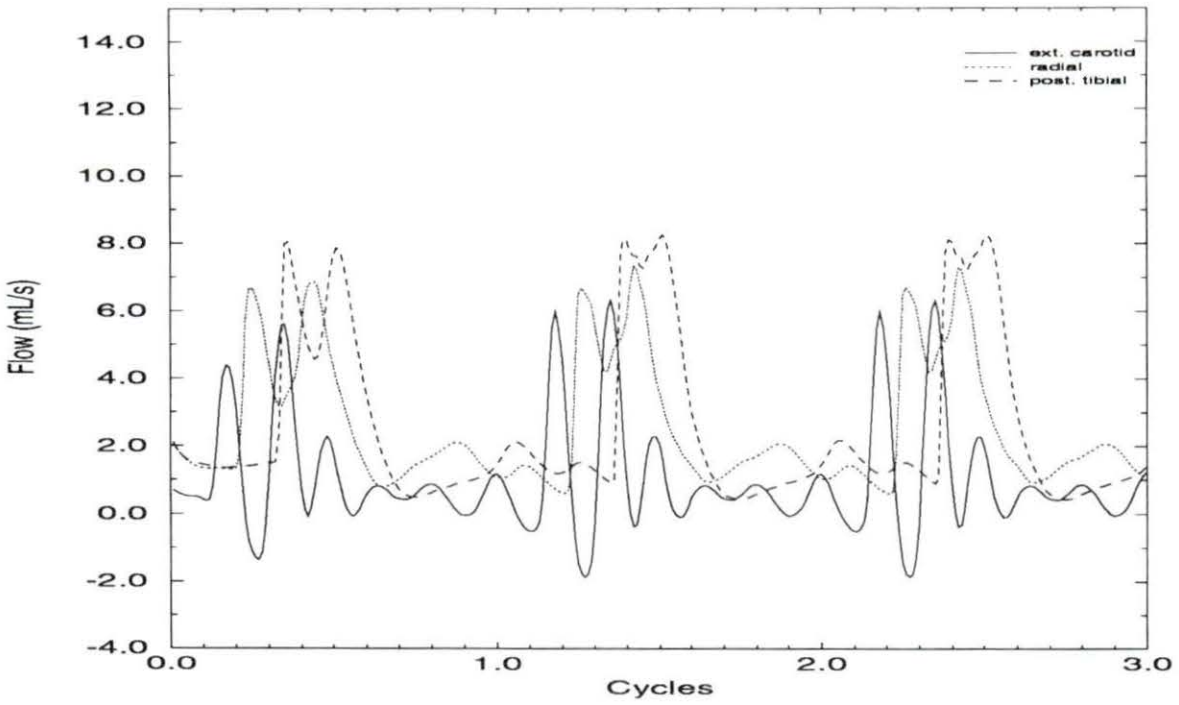

Figure 5.26: Flow pulses measured at various locations for AS/AI.

hypertension, all the index values have a minimum percent change of 69% in the external carotid artery, 54% in the radial artery, and 44% in the posterior tibial artery. The PI_f index seems to be the most sensitive to hypertension with ACI being a close second, especially as the pulse proceeds down the arterial tree.

Valvular Aortic Stenosis Patients with valvular aortic stenosis have heart rates of approximately 65 beats/min. The maximum and minimum flow (back flow) of all flow waveforms is decreased dramatically while the end diastolic flow magnitudes decrease only slightly from the normal flow. As in the hypertensive case, the increase of the slope along systolic flow is less steep, and the systolic phase lasts longer for AS than for the normal case. The index that would generally seem to be most sensitive to this diseased condition is ACI since the values measured for this index

change the most from the control values. From the index tables for the neck, the indices most dramatically affected are PI_f and ACI which decreased by 65% and 60% from control, respectively. The normalized PI_s value is greater than the control case which may be due to the the end diastolic flow being decreased the same magnitude in relation to the maximum flow. If the end diastolic flow were approximately the same as the control value, then the PI_s index would have decreased 46% from control and would have been more in line with the other indices all of which decreased by approximately $40\% \pm 5\%$ from control. For the wrist and ankle, the ACI index seems to be particularly affected by the heart condition, decreasing by 75% from control at the wrist and 50% from control at the ankle. All other indices varied less than 55% from control at the wrist and 40% from control at the ankle. Also, PI and PI_f appear to decrease as the pulse moves toward the periphery.

Pure Aortic Regurgitation The heart disease condition of pure aortic regurgitation increases heart rate to approximately 98 beats/min to compensate for the blood that flows backward through the incompetent heart valve. Other results of aortic regurgitation are an increase in the magnitude of all maximum, minimum, and end diastolic flows, and a decrease in time between end diastole and peak systole, resulting in a steeper slope. Aortic regurgitation would be expected to have the most dramatic effect on PI_s and ACI since they are calculated from values that have changed the most from the control values. From the index tables, all index values increase at the neck, especially the PI_s index. This may be due to the fact that the end diastolic flow value is very small compared to the control value. For the wrist, PI_s again varies the largest (83%) from control with PI_f varying the second largest

percentage at 33%. The indices calculated at the ankle react similarly to the way they reacted in the carotid, with PI_s and ACI deviating the most from control at 38%.

Combination of Aortic Stenosis and Regurgitation A combination of valvular aortic stenosis and aortic regurgitation exhibit an elevated heart rate of 84 beats/min. The aortic flow waveform is rather peculiar in that there is an extra hump after systolic flow. This is typical of the waveform of this type of patient. The values of mean flow and pressure in this case are quite high compared to the normal case. The aortic flow waveform shows an large increase in peak positive flow and in the end diastolic value, a slight increase in maximum back flow, a slight decrease in the systolic slope, and a very large increase in systolic duration. As the pulse proceeds down the arterial tree, the maximum flow and end diastolic flow decrease and eventually are less than the control case values. From the index tables for the case of combined aortic stenosis and regurgitation, the indices increase and decrease different amounts at different points on the body. PI_f appears to generally be the most sensitive to this waveform, varying by as much as 91% from control at the wrist and at least by 50%. The least sensitive index appears to be PI_s. This would be accurate since the maximum flow decreases approximately the same percentage as the end diastolic flow.

By examining the waveforms as well as inspecting the indices at a particular point in the body, a patient could be diagnosed with either a stenosis or heart ailment with a high percentage of confidence. The severity of stenosis could also be determined. Again, each index should be used with discretion since each index is a measure of

different waveform values to describe different traits. When used in combination, they could resolve an unclear heart disease diagnosis.

CHAPTER 6. CONCLUSIONS

In this study, a non-linear computer model of most of the human systemic circulation has been adapted and modified with the goal to examine the effects of arterial stenosis and, more importantly, various heart diseases on various flow indices. The modifications made to the model included a new compliance relationship to improve emulation of arterial compliance and nodal wall shear coefficient calculations throughout the arterial tree. Aortic pressure waveforms were used for the proximal boundary condition rather than a flow input since aortic pressure inputs for various cases of heart disease were readily available. Flow waveform indices designed to detect changes in certain properties of the waveform, such as minimum, maximum, and average flow values, were incorporated to measure the gross changes in the flow patterns of severe stenoses and heart diseases and were examined as a way of detecting such arterial and aortic diseases early on. Thus, flow indices could prove beneficial as a non-invasive diagnostic tool in a clinical environment. The computational model could also be used as an instructional aid to show the effects of varying different hemodynamic parameters for comparison with the results of in vivo experiments.

Such parameters as the type of proximal boundary condition used and varying wall shear coefficients rather than keeping them constant were given much consideration as to how they affected index sensitivity since they were not investigated in

previous studies with this model and indices. It was determined that wall shear coefficients make a difference on the indices calculated in this paper and that the type of proximal boundary condition did not. The indices chosen to study in the case of stenoses were the pulsatility index (PI), Fourier pulsatility index (PI_f), systolic-to-diastolic flow index (PI_s), acceleration index (ACI), and segmental systolic flow index (ARI). Each decreased with increasing stenosis severity as expected. When applied to the heart disease cases of hypertension, HYP, valvular aortic stenosis, AS, pure aortic regurgitation, AI, and a combination of aortic stenosis and regurgitation, AS/AI, the indices gave varying results based on how each was defined. Generally, PI_f and ACI were most consistently sensitive for hypertension and aortic stenosis, PI_s was generally most sensitive for aortic regurgitation, and PI_f was generally the most sensitive index for AS/AI. Each particular index would at times vary greatly depending on the point at which it was measured since each waveform shape is different. For instance, PI_f fluctuated from 50% above control at the external carotid, to 70% below control at the right radial artery, then to 90% above control at the posterior tibial artery for AS/AI. Thus, one must avoid hastily diagnosing a disease from a particular flow waveform at only one location in the body.

Recommendations

There are several improvements that could be made to the program as well as to make the model more valid.

- More peripheral arterial segments could be included in the model. Venous and cardiac dynamics could be included to make the model a closed loop system which would result in fewer deviations between experimental and simulated

pressure and flow waveforms.

- The physiological effects that various heart diseases have on autoregulation when a stenosis is present could be investigated and possibly modeled.

- A point-and-click style of user interaction to easily access data could be incorporated. A pictoral representation of all the arterial segments could be produced with all the segments numerically labeled. Upon using a mouse to point and click on a segment, a description of that segment would be produced, including a graphical display of pressure and flow running in real time. Comparative graphs of various cases could then be overlayed.

BIBLIOGRAPHY

Anliker, M., R. L. Rockwell, and E. Ogden. (1971). Nonlinear analysis of flow pulses and shock waves in arteries. *ZAMP*, Vol. 22, pp. 217–246.

Anliker, M., J. C. Stettler, P. Niederer, and R. Holenstein. (1978). Prediction of shape changes of propagation of flow and pressure pulses in human arteries. *The arterial system: Dynamics, control theory, and regulation*, pp. 15–34.

Aperia, A. (1940). Hemodynamical studies. *Skand. Arch. Physiol. Suppl.*, Vol. 83, pp. 1–230.

Archie, J. P. (1981). A simple, non-dimensioinal normalized common carotid doppler velocity wave-form index that idnetifies patients with carotid stenosis. *Stroke*, Vol.12, pp. 322–324.

Balar, S. D., T. R. Rogge, and D. F. Young. (1989). Computer simulation of blood flow in the human arm. *J. Biomechanics*, Vol. 22, pp. 691–697.

Bergel, D. H. (1961). The static elastic properties of the arterial wall. *J. Physiol.*, Vol. 156, pp. 445–457.

Fox, E. A., and E. Saibel. (1965). A formulation of the problem of flow through tubes. *Proceedings 4th International Congress on Rheology*, Vol. 4, pp. 125–133.

Frank, O. (1899). Die grunform des arterielennen pulses. Erste abhandlung. Mathematische analyse. *Z. Biol.*, Vol. 37, pp. 483-526.

Fronek, A., K. H. Johansen, R. B. Dilley, and E. F. Bernstein. (1973). Noninvasive physiologic tests in the diagnosis and characterization of peripheral arterial occlusive disease. *The American Journal of Surgery*, Vol.126, pp. 205–214.

Ganong, W. F. (1991). *Review of Medical Physiology.* 15th ed. Appleton and Lange, Norwalk, Connecticut.

Gosling, R. G., G. Dunbar, D. H. King, D. L. Newman, C. D. Side, J. P. Woodcock, D. E. Fitzgerald, J. S. Keates, and D. MacMillan. (1971). The quantitative analysis of occlusive peripheral arterial disease by a non-intrusive ultrasonic technique. *Angiology*, Vol. 22, pp. 52–55.

Gosling, R. G., and D. H. King. (1974). Continuous wave ultrasound as an alternative and complement to x-rays in vascular examinations. *Cardiovascular Applications of Ultrasound.* Reneman, Amsterdam.

Johnston, K. W., and I. Taraschuk. (1976). Validation of the role of pulsatility index in quantitation of the of the severity of peripheral arterial occlusive disease. *The American Journal of Surgery*, Vol. 131, pp. 295–297.

Johnston, K. W., B. C. Maruzzo, and R. S. C. Cobbold. (1978). Doppler methods for quantitative measurement and localization of peripheral arterial occlusive disease by analysis of the blood flow velocity waveform. *Ultrasound in Med. & Biol.*, Vol. 4, pp. 209–223.

Langewouters, G. J., K. H. Wesseling, and W. J. A. Goedhard. (1984). The static elastic properties of 45 human thoracic and 20 abdominal aortas in vitro and the parameters of a new model. *J. Biomech.*, Vol. 17, pp. 425–435.

Ling, S. C., B. H. Atabek, D. L. Fry, D. J. Patel, and J. S. Janicki. (1968). Aplication of heated-film velocity and shear probes to hemodynamic studies. *Circilat. Res.*, Vol. 23, pp. 789–801.

Manor, D., S. Sideman, U. Dinnar, R. Beyar. (1994). Analysis of coronary circulation under ischaemic conditions. *Electrocardiography*, Vol. 32, pp. 123–132.

Mason, D. T., E. Braunwald, J. Ross, and A. G. Morrow. (1964). Diagnostic value of the first and second derivatives of the arterial pressure pulse in the aortic valve disease and in hypertrophic subaortic stenosis. *Circulation*, Vol. 30, pp. 90–100.

McDonald, D. A. (1974). Blood flow in arteries. 2nd ed. Williams and Wilkins Co., Baltimore.

Morgan, G. W., and J. P. Kiely. (1954). Wave propagation in a viscous liquid contained in a flexible tube. *J. Acoust. Soc. Am.*, Vol. 26, pp.323–328.

Mozersky, D. J., D. S. Sumner, D. E. Hokanson, and D. E. Strandness, Jr. (1972). Transcutaneous measurement of the elastic properties of the human femoral artery. *Circulation*, Vol. 46, pp. 948–955.

Nichols, W. W., C. R. Conti, W. E. Walker, and W. R. Milnor. (1977). Input impedance of the systemic circulation in man. *Circ. Res.*, Vol. 40, pp. 451–458.

Noordergraaf, A., P. D. Verdouw, and H. B. C. Boom. (1963). The use of an analog computer in a circulation model. *Prog. Card. Diseases*, Vol. 5, pp. 419–439.

Pourcelot, L. (1974). Applications cliniques de l'examen Doppler transcutane. *Colloques ds l'Institute National de la Sante' et de la Recherche Medicale*, Vol 34, pp. 213–240.

Porenta, G. (1982). A computer based feasibility analysis of assessing arterial flow using pulsatility indices. M.S. Thesis. Iowa State University, Ames.

Porenta, G. P., D. F. Young, and T. R. Rogge. (1986). A finite-element model of blood flow in arteries including taper, branches, and obstructions. *J. Biomech. Engng*, Vol. 108, pp. 161–167.

Raines, J. K., M. Y. Jaffrin, and A. H. Shapiro. (1974). A computer simulation of arterial dynamics in the human leg. *J. Biomechanics*, Vol. 7, pp. 77–91.

Rangarajan, N. (1983). Estimation of cardiovascular system parameters using noninvasive measurements. Ph. D. Thesis. Iowa State University, Ames.

Rockwell, R. L., M. Anliker, and J. Elsner. (1974). Model studies of the pressure and flow pulses in viscoelastic arterial conduit. *J. Franklin Inst.*, Vol. 297, pp. 405–428.

Roederer, G. O., Y. E. Langlois, A. W. Chan, J. Primozich, R. J. Lawrence, P. M. Chikos, and D. E. Strandness Jr.. Ultrasound duplex scanning of the extracranial carotid arteries: improved accuracy using new features from the common carotid artery. *J. Cardiovascular Ultrasonography*, Vol.1, pp. 373–379.

Rooz, E. (1980). A finite element simulation of pulsatile flow in flexible tubes. Ph. D. Thesis. Iowa State University, Ames.

Rooz, E., D. F. Young, and T. R. Rogge. (1982). A finite element simulation of pulsatile flow in flexible obstructed tubes. *J. Biomechanical Eng.*, Vol. 104, pp. 119–124.

Rumberger, J. A., and R. M. Nerem. (1977). Method-of-characteristics calculation of coronary blood flow. *J. Fluid Mech.*, Vol. 32, pp. 429–448.

Schaaf, B. W., and P. H. Abbrecht. (1972). Digital computer simulation of human systemic arterial pulse transmission: A non-linear model. *J. Biomechanics*, Vol. 5, pp. 345–364.

Seeley, B. D., and D. F. Young. (1976). Effect of geometry on pressure losses across models of arterial stenosis. *J. Biomechanics*, Vol. 5, pp. 345–364.

Skalak, R. (1972). Synthesis of a complete circulation. *Cardiovascular Fluid Mechanics*, pp. 341–376.

Snyder, M. F., V. C. Rideout, and R. J. Hillestead. (1968). Computer modeling of the human systemic arterial tree. *J. Biomechanics*, Vol. 1, pp. 341–353.

Stergiopulos, N., D. F. Young, and T. R. Rogge. (1992). Computer simulation of arterial flow. *J. Biomechanics*, Vol. 25, pp. 1477–1488.

Stergiopulos, N., D. F. Young, and T. R. Rogge. (1993). Modeling the effect of arterial stenoses on flow and pressure waveforms. *ASME 1993 Advances in Bioengineering*, Vol. 26, pp. 451–453.

Stergiopulos, N., J. J. Meister, and N. Westerhof. (1994). Simple and accuraate way for estimating total and segmental arterial compliance: The pulse pressure method. *Annals of Biomedical Engineering*, Vol. 22, pp. 392–397.

Streeter, V. L., W. F. Keitzer, and D. F. Bohr. (1963). Pulsatile pressure and flow through distensible vessels. *Circ. Res. Vol.*, Vol. 13, pp. 3–20.

Uchida, S. (1956). The pulsating viscous flow superposed on steady laminar motion of incompressible fluid in a circular pipe. *ZAMP*, Vol. 7, pp. 403–421.

Weerappuli, D. P. V. (1987). Simulation of pulsatile flow in arteries using the finite-element method. Ph. D. Thesis. Iowa State University, Ames.

Wemple, R. R., and L. F. Mockros. (1972). Pressure and flow in the systemic arterial system. *J. Bimechanics*, Vol. 5, pp. 629–641.

Westerhof, N., F. Bosman, C. J. De Vries, and A. Noordergraaf. (1969). Analog studies of the human systemic arterial tree. *J. Biomechanics*, Vol. 2, pp. 121–143.

Witzig, K. (1914). Uber erzwungene Wellenbuewegungen zaher, inkompressibler Flussigkeitan in ilastischen Rohren. Inaugural Dissertation: Universitat Bern. Wyss Erben, Bern.

Womersley, J. R. (1955a). Method for the calculation of velocity, rate of flow, and viscous drag in arteries when the pressure gradient is known. *J. Physiol.*, Vol. 127, pp. 553–563.

Womersley, J. R. (1955b). Oscillatory motion of a viscous liquid in a thin-walled elastic tube. I. The linear approximation for long waves. *Phil. Mag.*, Vol. 46, pp. 199–221.

Womersley, J. R. (1957). The mathematical analysis of the arterial circulation in a state of oscillatory motion. Wright Air Development Center, *WADC Technical Report TR*, pp. 56–614.

Young, D. F., and F. Y. Tsai. (1973a). Flow characterisitcs in models of arterial stenoses. I. Steady Flow. *J. Biomechanics*, Vol. 6, pp.395–410.

Young, D. F., and F. Y. Tsai. (1973b). Flow characterisitcs in models of arterial stenoses. II. Unsteady Flow. *J. Biomechanics*, Vol. 6, pp.547–559.

Young, D. F., N. R. Cholvin, and A. C. Roth. (1975). Pressure drop across artificially induced stenoses in the femoral arteries of dogs. *Circ. Res.*, Vol. 36, pp. 735–743.

Young, D. F. (1979). Fluid mechanics of arterial stenosis. *J. Biomechanical Eng.*, Vol. 101, pp. 157–175.

Young, D. F., T. R. Rogge, T. A. Gray, and E. Rooz. (1980). Indirect evaluation of systemic parameters for pulsatile flow in flexible tubes. *J. Biomechanics*, Vol. 5, pp. 339–347.

APPENDIX A. SAMPLE INPUT DATA – CONTROL CASE

NUMBER OF SEGMENTS
55

SEG#	BRAN	PARNT	STN	#NOD	SEGMT LENGTH	INPUT AREA	OUTPUT AREA
1	2	0	0	2	4.00000E-2	6.78866E-4	6.51440E-4
2	14	1	0	2	2.00000E-2	3.94081E-4	3.94081E-4
3	4	1	0	3	3.40000E-2	1.20763E-4	1.20763E-4
4	6	3	0	3	3.40000E-2	5.62122E-5	5.10223E-5
5	12	3	0	5	1.77000E-1	4.30084E-5	4.30084E-5
6	0	4	0	5	1.48000E-1	1.11036E-5	1.05209E-5
7	8	4	0	9	4.22000E-1	5.10222E-5	1.74974E-5
8	0	7	0	6	2.35000E-1	9.51148E-6	6.33470E-6
9	10	7	0	4	6.70000E-2	1.45220E-5	1.29462E-5
10	0	9	0	4	7.90000E-2	2.60155E-6	2.60155E-6
11	0	9	0	5	1.71000E-1	1.29462E-5	1.05209E-5
12	0	5	0	5	1.77000E-1	9.84229E-6	2.16424E-6
13	0	5	0	5	1.77000E-1	9.84229E-6	2.16424E-6
14	18	2	0	2	3.90000E-2	3.59681E-4	3.59681E-4
15	16	2	0	6	2.08000E-1	4.30084E-5	4.30084E-5
16	0	15	0	5	1.77000E-1	9.84229E-6	2.16424E-6
17	0	15	0	5	1.77000E-1	9.84229E-6	2.16424E-6
18	26	14	0	3	5.20000E-2	3.13531E-4	1.43139E-4
19	20	14	0	2	3.40000E-2	5.62122E-5	5.10223E-5
20	0	19	0	5	1.48000E-1	1.11036E-5	1.05209E-5
21	22	19	0	9	4.22000E-1	5.10222E-5	1.74974E-5
22	0	21	0	6	2.35000E-1	9.51148E-6	6.33470E-6
23	24	21	0	4	6.70000E-2	1.45220E-5	1.29462E-5
24	0	23	0	4	7.90000E-2	2.60155E-6	2.60155E-6
25	0	23	0	5	1.71000E-1	1.29462E-5	1.05209E-5

26	0	18	0	4	8.00000E-2	1.25664E-5	7.06858E-6
27	28	18	0	5	1.04000E-1	1.43139E-4	1.16899E-4
28	34	27	0	3	5.30000E-2	1.16899E-4	1.05683E-4
29	30	27	0	2	1.00000E-2	4.77836E-5	4.77836E-5
30	32	29	0	2	1.00000E-2	4.77836E-5	4.77836E-5
31	0	29	0	3	6.60000E-2	1.52053E-5	1.52053E-5
32	0	30	0	3	7.10000E-2	1.01788E-5	1.01788E-5
33	0	30	0	3	6.30000E-2	2.37583E-5	2.37583E-5
34	0	28	0	4	5.90000E-2	5.94467E-5	5.94467E-5
35	36	28	0	2	1.00000E-2	1.05683E-4	1.04586E-4
36	0	35	0	2	3.20000E-2	2.12371E-5	2.12371E-5
37	38	35	0	2	1.00000E-2	1.04586E-4	1.03494E-4
38	0	37	0	2	3.20000E-2	2.12371E-5	2.12371E-5
39	40	37	0	5	7.06000E-2	1.03494E-4	9.53856E-5
40	0	39	0	3	5.00000E-2	8.04247E-6	8.04247E-6
41	42	39	0	2	1.00000E-2	9.53856E-5	9.43433E-5
42	44	41	0	3	5.82000E-2	4.25447E-5	3.69605E-5
43	50	41	0	3	5.82000E-2	4.25447E-5	3.69605E-5
44	46	42	0	4	1.44000E-1	3.69605E-5	2.29022E-5
45	0	42	0	3	5.00000E-2	1.25660E-5	1.25660E-5
46	48	44	0	9	4.43000E-1	2.29022E-5	1.13411E-5
47	0	44	0	4	1.26000E-1	2.04282E-5	1.08686E-5
48	0	46	0	8	3.21000E-1	1.01788E-5	6.24580E-6
49	0	46	0	8	3.43000E-1	5.30929E-6	3.14159E-6
50	52	43	0	4	1.44000E-1	3.69605E-5	2.29022E-5
51	0	43	0	3	5.00000E-2	1.25660E-5	1.25660E-5
52	54	50	0	9	4.43000E-1	2.29022E-5	1.13411E-5
53	0	50	0	4	1.26000E-1	2.04282E-5	1.08686E-5
54	0	52	0	8	3.21000E-1	1.01788E-5	6.24580E-6
55	0	52	0	8	3.43000E-1	5.30929E-6	3.14159E-6

SEG#	COMPLIANCE	SEEPAGE	ORIENTATION ANGLE
1	2.61000D-08	0.00000D+0	0.09000D+3
2	1.48000D-08	0.00000D+0	0.00000D+3
3	3.97059D-09	0.00000D+0	0.13500D+3
4	1.64706D-09	0.00000D+0	0.18000D+3
5	1.20678D-09	0.00000D+0	0.09000D+3
6	1.13649D-10	0.00000D+0	0.12000D+3
7	8.02607D-10	0.00000D+0	0.24000D+3
8	7.98723D-11	0.00000D+0	0.24000D+3

9	1.65672D-10	0.00000D+0	0.24000D+3
10	1.13924D-11	0.00000D+0	0.24000D+3
11	1.29240D-10	0.00000D+0	0.24000D+3
12	5.32768D-11	0.00000D+0	0.09000D+3
13	5.32768D-11	0.00000D+0	0.13500D+3
14	1.33590D-08	0.00000D+0	0.00000D+3
15	1.20673D-09	0.00000D+0	0.06000D+3
16	5.32768D-11	0.00000D+0	0.09000D+3
17	5.32768D-11	0.00000D+0	0.04500D+3
18	1.14808D-08	0.00000D+0	0.27000D+3
19	1.64706D-09	0.00000D+0	0.04500D+3
20	1.13649D-10	0.00000D+0	0.06000D+3
21	8.02607D-10	0.00000D+0	0.30000D+3
22	7.98723D-11	0.00000D+0	0.30000D+3
23	1.65670D-10	0.00000D+0	0.30000D+3
24	1.13920D-11	0.00000D+0	0.30000D+3
25	1.29240D-10	0.00000D+0	0.30000D+3
26	3.75000D-10	0.00000D+0	0.00000D+3
27	4.57690D-09	0.00000D+0	0.27000D+3
28	3.84906D-09	0.00000D+0	0.27000D+3
29	1.36000D-09	0.00000D+0	0.00000D+3
30	1.00000D-09	0.00000D+0	0.00000D+3
31	3.48485D-10	0.00000D+0	0.31500D+3
32	2.12676D-10	0.00000D+0	0.45000D+3
33	5.93651D-10	0.00000D+0	0.00000D+3
34	1.76271D-09	0.00000D+0	0.22500D+3
35	4.00000D-09	0.00000D+0	0.27000D+3
36	5.21875D-10	0.00000D+0	0.00000D+3
37	3.80000D-09	0.00000D+0	0.27000D+3
38	5.21875D-10	0.00000D+0	0.00000D+3
39	3.19811D-09	0.00000D+0	0.27000D+3
40	1.58400D-10	0.00000D+0	0.27000D+3
41	3.50000D-09	0.00000D+0	0.27000D+3
42	7.86942D-10	0.00000D+0	0.31500D+3
43	7.86942D-10	0.00000D+0	0.22500D+3
44	1.08472D-09	0.00000D+0	0.31500D+3
45	6.60000D-10	0.00000D+0	0.27000D+3
46	3.07901D-10	0.00000D+0	0.27000D+3
47	8.96825D-11	0.00000D+0	0.31500D+3
48	6.87227D-11	0.00000D+0	0.27000D+3

49	2.45481D-11	0.00000D+0	0.27000D+3
50	1.08472D-09	0.00000D+0	0.22500D+3
51	6.60000D-10	0.00000D+0	0.27000D+3
52	3.07901D-10	0.00000D+0	0.27000D+3
53	8.96825D-11	0.00000D+0	0.22500D+3
54	6.87227D-11	0.00000D+0	0.27000D+3
55	2.45481D-11	0.00000D+0	0.27000D+3

SEG	RES1	RES2	CT
6	.12020E+10	.48080E+10	.30955E-10
8	.10560E+10	.42240E+10	.35235E-10
10	.16860E+11	.67440E+11	.22069E-11
11	.10560E+10	.42240E+10	.35235E-10
12	.27800E+10	.11120E+11	.13384E-10
13	.27800E+10	.11120E+11	.13384E-10
16	.27800E+10	.11120E+11	.13384E-10
17	.27800E+10	.11120E+11	.13384E-10
20	.12020E+10	.48080E+10	.30955E-10
22	.10560E+10	.42240E+10	.35235E-10
24	.16860E+11	.67440E+11	.22069E-11
25	.10560E+10	.42240E+10	.35235E-10
26	.27800E+09	.11120E+10	.13384E-09
31	.72600E+09	.29040E+10	.51251E-10
32	.10820E+10	.43280E+10	.34389E-10
33	.46400E+09	.18560E+10	.80191E-10
34	.18600E+09	.74400E+09	.20005E-09
36	.22600E+09	.90400E+09	.16464E-09
38	.22600E+09	.90400E+09	.16464E-09
40	.13760E+10	.55040E+10	.27041E-10
45	.15872E+10	.63488E+10	.23443E-10
47	.95400E+09	.38160E+10	.39003E-10
48	.95400E+09	.38160E+10	.39003E-10
49	.11180E+10	.44720E+10	.33281E-10
51	.15872E+10	.63488E+10	.23443E-10
53	.95400E+09	.38160E+10	.39003E-10
54	.95400E+09	.38160E+10	.39003E-10
55	.11180E+10	.44720E+10	.33281E-10

DENSITY	VISCOSITY
0.10500D+4	0.45000D-2

CYCLES	FREQUENCY	TIME INCREMENT
3	1.00000D00	0.50000D-3

NPB	NQB
0	21

Q COS TERM	Q SIN TERM
0.86393E-4	0.00000E+0
-.88455E-4	0.13368E-3
-.52515E-4	-.12280E-3
0.86471E-4	0.22459E-4
-.26395E-4	0.22693E-4
-.12987E-4	0.22398E-5
0.20133E-5	-.22315E-4
0.70896E-5	0.10065E-4
0.32577E-5	-.21066E-5
-.56573E-5	0.90633E-5
-.19302E-5	-.85422E-5
0.22387E-5	0.14770E-5
0.23050E-5	-.32397E-5
0.11909E-5	0.59775E-5
-.39818E-5	-.18464E-5
0.58176E-6	-.14751E-5
0.19556E-5	-.12112E-5
0.48907E-6	0.24434E-5
-.66338E-6	0.50967E-6
-.21719E-5	-.23241E-6
0.19705E-5	-.20190E-5

ACC. GRAV.	GRAV. LOAD	ANGLE
9.81000D00	0.00000D+0	0.27000D+3

APPENDIX B. SAMPLE INPUT DATA – 90% STENOSIS IN LEFT FEMORAL ARTERY

NUMBER OF SEGMENTS
55

SEG#	BRAN	PARNT	STN	#NOD	SEGMT LENGTH	INPUT AREA	OUTPUT AREA
1	2	0	0	2	4.00000E-2	6.78866E-4	6.51440E-4
2	14	1	0	2	2.00000E-2	3.94081E-4	3.94081E-4
3	4	1	0	3	3.40000E-2	1.20763E-4	1.20763E-4
4	6	3	0	3	3.40000E-2	5.62122E-5	5.10223E-5
5	12	3	0	5	1.77000E-1	4.30084E-5	4.30084E-5
6	0	4	0	5	1.48000E-1	1.11036E-5	1.05209E-5
7	8	4	0	9	4.22000E-1	5.10222E-5	1.74974E-5
8	0	7	0	6	2.35000E-1	9.51148E-6	6.33470E-6
9	10	7	0	4	6.70000E-2	1.45220E-5	1.29462E-5
10	0	9	0	4	7.90000E-2	2.60155E-6	2.60155E-6
11	0	9	0	5	1.71000E-1	1.29462E-5	1.05209E-5
12	0	5	0	5	1.77000E-1	9.84229E-6	2.16424E-6
13	0	5	0	5	1.77000E-1	9.84229E-6	2.16424E-6
14	18	2	0	2	3.90000E-2	3.59681E-4	3.59681E-4
15	16	2	0	6	2.08000E-1	4.30084E-5	4.30084E-5
16	0	15	0	5	1.77000E-1	9.84229E-6	2.16424E-6
17	0	15	0	5	1.77000E-1	9.84229E-6	2.16424E-6
18	26	14	0	3	5.20000E-2	3.13531E-4	1.43139E-4
19	20	14	0	2	3.40000E-2	5.62122E-5	5.10223E-5
20	0	19	0	5	1.48000E-1	1.11036E-5	1.05209E-5
21	22	19	0	9	4.22000E-1	5.10222E-5	1.74974E-5
22	0	21	0	6	2.35000E-1	9.51148E-6	6.33470E-6
23	24	21	0	4	6.70000E-2	1.45220E-5	1.29462E-5

24	0	23	0	4	7.90000E-2	2.60155E-6	2.60155E-6
25	0	23	0	5	1.71000E-1	1.29462E-5	1.05209E-5
26	0	18	0	4	8.00000E-2	1.25664E-5	7.06858E-6
27	28	18	0	5	1.04000E-1	1.43139E-4	1.16899E-4
28	34	27	0	3	5.30000E-2	1.16899E-4	1.05683E-4
29	30	27	0	2	1.00000E-2	4.77836E-5	4.77836E-5
30	32	29	0	2	1.00000E-2	4.77836E-5	4.77836E-5
31	0	29	0	3	6.60000E-2	1.52053E-5	1.52053E-5
32	0	30	0	3	7.10000E-2	1.01788E-5	1.01788E-5
33	0	30	0	3	6.30000E-2	2.37583E-5	2.37583E-5
34	0	28	0	4	5.90000E-2	5.94467E-5	5.94467E-5
35	36	28	0	2	1.00000E-2	1.05683E-4	1.04586E-4
36	0	35	0	2	3.20000E-2	2.12371E-5	2.12371E-5
37	38	35	0	2	1.00000E-2	1.04586E-4	1.03494E-4
38	0	37	0	2	3.20000E-2	2.12371E-5	2.12371E-5
39	40	37	0	5	7.06000E-2	1.03494E-4	9.53856E-5
40	0	39	0	3	5.00000E-2	8.04247E-6	8.04247E-6
41	42	39	0	2	1.00000E-2	9.53856E-5	9.43433E-5
42	44	41	0	3	5.82000E-2	4.25447E-5	3.69605E-5
43	50	41	0	3	5.82000E-2	4.25447E-5	3.69605E-5
44	46	42	0	4	1.44000E-1	3.69605E-5	2.29022E-5
45	0	42	0	3	5.00000E-2	1.25660E-5	1.25660E-5
46	48	44	4	9	4.43000E-1	2.29022E-5	1.13411E-5
47	0	44	0	4	1.26000E-1	2.04282E-5	1.08686E-5
48	0	46	0	8	3.21000E-1	1.01788E-5	6.24580E-6
49	0	46	0	8	3.43000E-1	5.30929E-6	3.14159E-6
50	52	43	0	4	1.44000E-1	3.69605E-5	2.29022E-5
51	0	43	0	3	5.00000E-2	1.25660E-5	1.25660E-5
52	54	50	0	9	4.43000E-1	2.29022E-5	1.13411E-5
53	0	50	0	4	1.26000E-1	2.04282E-5	1.08686E-5
54	0	52	0	8	3.21000E-1	1.01788E-5	6.24580E-6
55	0	52	0	8	3.43000E-1	5.30929E-6	3.14159E-6

SEG#	COMPLIANCE	SEEPAGE	ORIENTATION ANGLE
1	2.61000D-08	0.00000D+0	0.09000D+3
2	1.48000D-08	0.00000D+0	0.00000D+3
3	3.97059D-09	0.00000D+0	0.13500D+3
4	1.64706D-09	0.00000D+0	0.18000D+3
5	1.20678D-09	0.00000D+0	0.09000D+3
6	1.13649D-10	0.00000D+0	0.12000D+3

7	8.02607D-10	0.00000D+0	0.24000D+3
8	7.98723D-11	0.00000D+0	0.24000D+3
9	1.65672D-10	0.00000D+0	0.24000D+3
10	1.13924D-11	0.00000D+0	0.24000D+3
11	1.29240D-10	0.00000D+0	0.24000D+3
12	5.32768D-11	0.00000D+0	0.09000D+3
13	5.32768D-11	0.00000D+0	0.13500D+3
14	1.33590D-08	0.00000D+0	0.00000D+3
15	1.20673D-09	0.00000D+0	0.06000D+3
16	5.32768D-11	0.00000D+0	0.09000D+3
17	5.32768D-11	0.00000D+0	0.04500D+3
18	1.14808D-08	0.00000D+0	0.27000D+3
19	1.64706D-09	0.00000D+0	0.04500D+3
20	1.13649D-10	0.00000D+0	0.06000D+3
21	8.02607D-10	0.00000D+0	0.30000D+3
22	7.98723D-11	0.00000D+0	0.30000D+3
23	1.65670D-10	0.00000D+0	0.30000D+3
24	1.13920D-11	0.00000D+0	0.30000D+3
25	1.29240D-10	0.00000D+0	0.30000D+3
26	3.75000D-10	0.00000D+0	0.00000D+3
27	4.57690D-09	0.00000D+0	0.27000D+3
28	3.84906D-09	0.00000D+0	0.27000D+3
29	1.36000D-09	0.00000D+0	0.00000D+3
30	1.00000D-09	0.00000D+0	0.00000D+3
31	3.48485D-10	0.00000D+0	0.31500D+3
32	2.12676D-10	0.00000D+0	0.45000D+3
33	5.93651D-10	0.00000D+0	0.00000D+3
34	1.76271D-09	0.00000D+0	0.22500D+3
35	4.00000D-09	0.00000D+0	0.27000D+3
36	5.21875D-10	0.00000D+0	0.00000D+3
37	3.80000D-09	0.00000D+0	0.27000D+3
38	5.21875D-10	0.00000D+0	0.00000D+3
39	3.19811D-09	0.00000D+0	0.27000D+3
40	1.58400D-10	0.00000D+0	0.27000D+3
41	3.50000D-09	0.00000D+0	0.27000D+3
42	7.86942D-10	0.00000D+0	0.31500D+3
43	7.86942D-10	0.00000D+0	0.22500D+3
44	1.08472D-09	0.00000D+0	0.31500D+3
45	6.60000D-10	0.00000D+0	0.27000D+3
46	3.07901D-10	0.00000D+0	0.27000D+3

47	8.96825D-11	0.00000D+0	0.31500D+3
48	6.87227D-11	0.00000D+0	0.27000D+3
49	2.45481D-11	0.00000D+0	0.27000D+3
50	1.08472D-09	0.00000D+0	0.22500D+3
51	6.60000D-10	0.00000D+0	0.27000D+3
52	3.07901D-10	0.00000D+0	0.27000D+3
53	8.96825D-11	0.00000D+0	0.22500D+3
54	6.87227D-11	0.00000D+0	0.27000D+3
55	2.45481D-11	0.00000D+0	0.27000D+3

SEG	RES1	RES2	CT
6	.12020E+10	.48080E+10	.30955E-10
8	.10560E+10	.42240E+10	.35235E-10
10	.16860E+11	.67440E+11	.22069E-11
11	.10560E+10	.42240E+10	.35235E-10
12	.27800E+10	.11120E+11	.13384E-10
13	.27800E+10	.11120E+11	.13384E-10
16	.27800E+10	.11120E+11	.13384E-10
17	.27800E+10	.11120E+11	.13384E-10
20	.12020E+10	.48080E+10	.30955E-10
22	.10560E+10	.42240E+10	.35235E-10
24	.16860E+11	.67440E+11	.22069E-11
25	.10560E+10	.42240E+10	.35235E-10
26	.27800E+09	.11120E+10	.13384E-09
31	.72600E+09	.29040E+10	.51251E-10
32	.10820E+10	.43280E+10	.34389E-10
33	.46400E+09	.18560E+10	.80191E-10
34	.18600E+09	.74400E+09	.20005E-09
36	.22600E+09	.90400E+09	.16464E-09
38	.22600E+09	.90400E+09	.16464E-09
40	.13760E+10	.55040E+10	.27041E-10
45	.15872E+10	.63488E+10	.23443E-10
47	.95400E+09	.38160E+10	.39003E-10
48	.95400E+09	.38160E+10	.39003E-10
49	.11180E+10	.44720E+10	.33281E-10
51	.15872E+10	.63488E+10	.23443E-10
53	.95400E+09	.38160E+10	.39003E-10
54	.95400E+09	.38160E+10	.39003E-10
55	.11180E+10	.44720E+10	.33281E-10

SEG	X STENOSIS	STEN. LENGTH	%
46	.20000E+00	.02000E+00	.90000E+00

DENSITY	VISCOSITY
0.10500D+4	0.45000D-2

CYCLES	FREQUENCY	TIME INCREMENT
3	1.00000D00	0.50000D-3

NPB	NQB
0	21

Q COS TERM	Q SIN TERM
0.86393E-4	0.00000E+0
-.88455E-4	0.13368E-3
-.52515E-4	-.12280E-3
0.86471E-4	0.22459E-4
-.26395E-4	0.22693E-4
-.12987E-4	0.22398E-5
0.20133E-5	-.22315E-4
0.70896E-5	0.10065E-4
0.32577E-5	-.21066E-5
-.56573E-5	0.90633E-5
-.19302E-5	-.85422E-5
0.22387E-5	0.14770E-5
0.23050E-5	-.32397E-5
0.11909E-5	0.59775E-5
-.39818E-5	-.18464E-5
0.58176E-6	-.14751E-5
0.19556E-5	-.12112E-5
0.48907E-6	0.24434E-5
-.66338E-6	0.50967E-6
-.21719E-5	-.23241E-6
0.19705E-5	-.20190E-5

ACC. GRAV.	GRAV. LOAD	ANGLE
9.81000D00	0.00000D+0	0.27000D+3